JOURNAL OF PETROLOGY | VOLUME 47 | NUMBER 5 | PAGES 859–882 | 2006 | doi:10.1093/petrology/egi098

Beryllium and Other Trace Elements in Paragneisses and Anatectic Veins of the Ultrahigh-Temperature Napier Complex, Enderby Land, East Antarctica: the Role of Sapphirine

EDWARD S. GREW[1]*, MARTIN G. YATES[1], CHARLES K. SHEARER[2], JUSTIN J. HAGERTY[2], JOHN W. SHERATON[3] AND MICHAEL SANDIFORD[4]

[1]DEPARTMENT OF EARTH SCIENCES, UNIVERSITY OF MAINE, 5790 EDWARD T. BRYAND RESEARCH CENTER, ORONO, ME 04469-5790, USA

[2]INSTITUTE OF METEORITICS, UNIVERSITY OF NEW MEXICO, ALBUQUERQUE, NM 87131, USA

[3]STONEACRE, BREAM ROAD, ST. BRIAVELS, LYDNEY GL15 6TL UK

[4]SCHOOL OF EARTH SCIENCES, UNIVERSITY OF MELBOURNE, CARLTON, VIC. 3010, AUSTRALIA

RECEIVED SEPTEMBER 27, 2004; ACCEPTED DECEMBER 14, 2005
ADVANCE ACCESS PUBLICATION JANUARY 13, 2006

Anatectic veins containing the Be minerals khmaralite and beryllian sapphirine as primary phases (or surinamite derived therefrom) are associated with Mg–Al-rich paragneisses at three localities in the ultrahigh-temperature Napier complex, Antarctica, a unique Be mineralization in the granulite facies. Likely precursors of the paragneisses are volcaniclastic deposits that were hydrothermally altered by heated seawater prior to metamorphism. Regular distribution of Be among minerals in the paragneisses suggests an approach to equilibrium with Be greatly concentrated in sapphirine (25–3430 ppm Be) or cordierite (560–930 ppm Be) relative to plagioclase An53–66 (14–43 ppm Be) > cores of coarse-grained orthopyroxene (0·7–29 ppm Be) > coronitic orthopyroxene (0·4–14 ppm Be) ≈ sillimanite (0·1–26 ppm Be) ≈ plagioclase An18–33 (0·6–15 ppm Be) > biotite (0·06–8 ppm Be) > K-feldspar, quartz, garnet (0·05–0·7 ppm Be). Sapphirine-bearing paragneisses have average Be concentrations, 4·9 ± 2·4 ppm (13 samples), about twice that of typical pelites, whereas paragneisses lacking sapphirine and primary cordierite have only 2·9 ± 2·1 ppm Be (12 samples), implying some loss of Be during metamorphism. The likely source rocks for the Be-rich melts were biotitic rocks lacking the Be sinks sapphirine and cordierite. These gneisses were probably less competent than the sapphirine-bearing gneisses, so the melts were drawn to the latter and collected in spaces opened during deformation and boudinage of the more competent paragneisses. Fractionation of the melts concentrated Be to the extent that Be minerals could crystallize. The final result was Be-mineralized anatectic veins hosted by relatively Be-rich sapphirine-bearing paragneisses.

KEY WORDS: *Antarctica; beryllium; granulite facies; microprobe; sapphirine*

INTRODUCTION

Beryllium constitutes only 3 ppm of the Earth's upper continental crust (Taylor & McLennan, 1995), but through a combination of anatexis and crystal fractionation it is concentrated by two to three orders of magnitude in granitic pegmatites where beryllium minerals, most commonly beryl, are found (e.g. London & Evensen, 2002). Beryllium enrichment in granulite-facies rocks is rare,

*Corresponding author. Telephone: 207-581-2169. Fax: 207-581-2202. E-mail: esgrew@maine.edu

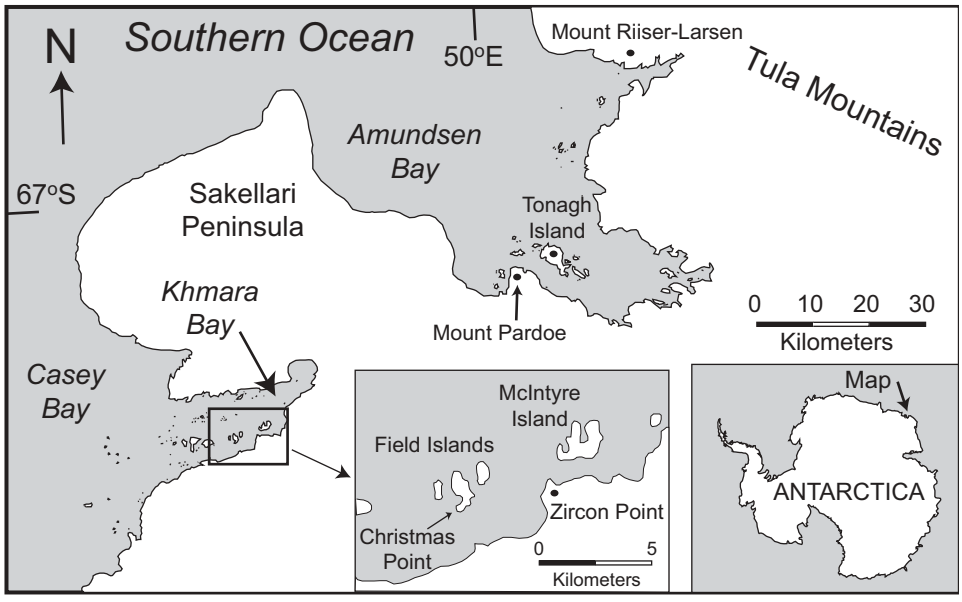

Fig. 1. Map of western Enderby Land, East Antarctica, showing the locations mentioned in the text [simplified from Sheraton *et al.* (1987)].

and the occurrence of high-temperature Be minerals in coarse-grained anatectic veins associated with sapphirine-bearing, quartz-rich paragneisses in the Archean Napier complex, Antarctica, is unique. These Be minerals are khmaralite, $(Mg,Fe^{2+})_{3{\cdot}5}(Al,Fe^{3+})_7BeSi_{2{\cdot}5}O_{20}$, which is an ordered derivitive of sapphirine-2*M* (Barbier *et al.*, 1999), and surinamite, $(Mg,Fe^{2+})_3(Al,Fe^{3+})_4BeSi_3O_{16}$, both high-temperature minerals requiring at least 650°C for synthesis (Hölscher *et al.*, 1986; Christy *et al.*, 2002), as well as magnesiotaaffeite-6*N*′3*S* ['musgravite', $(Mg,Fe,Zn)_2BeAl_6O_{12}$] and chrysoberyl (Grew, 1981, 1998; Grew *et al.*, 2000).

The present paper is an investigation of the Be budget of Napier Complex paragneisses containing sapphirine, orthopyroxene or sillimanite and their relation to the anatectic veins containing Be minerals. Our objective is to explain where the Be originated and how it was enriched in the veins. Typical pelitic rocks contain 3 ppm Be on average (Grew, 2002*b*), and formation of Be-enriched anatectic melts from such a Be-poor source involves extensive fractionation (Evensen & London, 2002, 2003; London & Evensen, 2002). According to Evensen & London, an important condition is that cordierite is absent in the source rock. More than any common rock-forming mineral cordierite concentrates Be relative to melt, so that if cordierite were a product of the melting reaction, the melt would be depleted in Be. Sapphirine is another mineral that strongly concentrates Be (e.g. Grew, 2002*b*), and thus melts derived from the anatexis of sapphirine-bearing rocks should also be depleted in Be. The presence of Be minerals in veins associated with sapphirine-bearing metasedimentary host-rocks thus appears to contradict the Evensen & London (2002, 2003) model. We use the results of the present study to reconcile the observed association with the Evensen & London model.

FIELD RELATIONSHIPS

The veins containing high-temperature Be minerals belong to a generation found sparingly throughout the Napier Complex. Measured ages range from 2450 to 2590 Ma (e.g. Black *et al.*, 1983; Grew, 1998; Harley, 2004). In Casey Bay (Fig. 1) this generation was emplaced during the main deformation D_2 or in its waning stages and at the peak of ultrahigh-temperature (UHT) metamorphism, or a relatively short time thereafter, and represents D_2 anatectic melts (Sandiford & Wilson, 1984, 1986). S. L. Harley (unpublished data, 2004) identified a generation of veins on Tonagh Island synchronous with D_2 (Hollis, 2000). The veins at Mount Pardoe probably belong to this generation, i.e. all the studied veins can be considered to be coeval, Late Archean melts.

The anatectic veins sampled for the present study appear in three distinct structural types: (1) cross-cutting pods up to a few meters long and up to 1·5 m thick at Christmas Point and Zircon Point (Casey Bay); (2) veins 5 cm thick at Mount Pardoe (Amundsen Bay); (3) inter-boudin pockets a few centimeters across at McIntyre Island (Casey Bay). The pods at Christmas Point constitute an en echelon array oriented at high angles to the compositional layering in the host paragneisses. The tectonic fabric in the host is warped in the vicinity of the pods (e.g. Fig. 2a); deformation in the pods is evident in

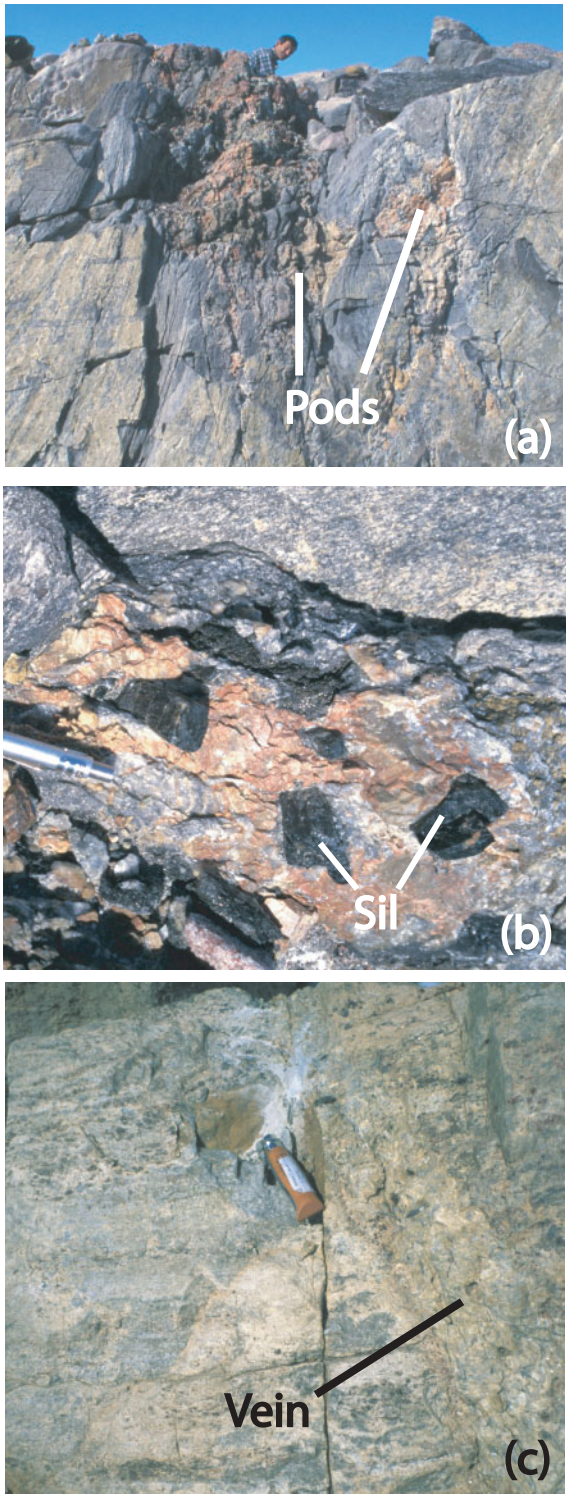

Fig. 2. Photographs of veins in the field [modified from Grew *et al.* (2000)]. (a) View roughly SE of pods containing red microcline in gray quartz-rich paragneiss at Christmas Point. Photograph is courtesy of Dan Dunkley. (b) Pod containing red microcline and coarse brown sillimanite prisms (Sil) in gray quartz-rich paragneiss at Christmas Point. Photograph is courtesy of Dan Dunkley. (c) Cross-cutting vein in block of paragneiss at Mount Pardoe.

the bending of sillimanite prisms and granulation of coarse-grained microcline. The red microcline in the pod emphasizes the distinction between the coarse-grained pod and medium-grained gray host paragneisses (Fig. 2b). There is no evidence of an aureole or mafic selvage around these pods. Seven of the 11 studied host quartz-rich paragneisses from Christmas Point (2292 series) were collected from the layer shown in Fig. 2a over a distance of 5 m across strike in the vicinity of a pod 1 m in size containing Be minerals (Grew *et al.*, 2000), whereas 2282G, R25517, R31238, and R31243 were collected within about 100 m.

The pod with Be minerals at Zircon Point is hosted by a layer of distinctive light-weathering quartz-rich paragneisses. Although microcline is yellow in this pod, the pod is distinct from the host paragneisses because it is coarse-grained and has slightly discolored the paragneiss. None of the analyzed paragneisses were collected from this particular layer. Samples 2234A, D, E were collected from another light-weathering layer, but cropping out a few tens of meters across strike. Samples 2234H, J were collected from different layers near the sampled light-weathering layer. Although orthopyroxene was noted only in the rocks hosting the pod, the overall similarity between the two layers is our justification for using the analyzed suite as a proxy for the paragneisses hosting the Be-bearing pod. C. J. L. Wilson collected sample R31050 from a light-weathering layer about 280 m north across strike.

All Mount Pardoe samples were collected from broken outcrops within an area not exceeding 10 m^2 (Grew *et al.*, 2000). In contrast to the pods at Christmas Point and Zircon Point, the veins are much less distinct in color and grain size from the host-rock, and tend to blend in with it; no discoloration or mafic selvage is evident along the contacts (Fig. 2c). The McIntyre Island quartz-rich paragneisses that host the studied interboudin pockets are represented by two specimens (Fig. 3a) from different localities on the island.

PETROGRAPHIC DESCRIPTION AND INTERPRETATION

Host paragneisses

Host-rocks at Christmas Point, Zircon Point, Mount Pardoe and McIntyre Island are predominantly quartz-rich paragneisses and contain sapphirine, sillimanite, orthopyroxene, and/or garnet (Table 1 and Grew *et al.*, 2000). With rare exception, sapphirine does not exceed a few modal per cent. Biotite is present in most thin sections, but generally in only trace or minor amounts. Most biotite could be secondary, i.e. a product resulting from crystallization of melts not driven out at the peak of

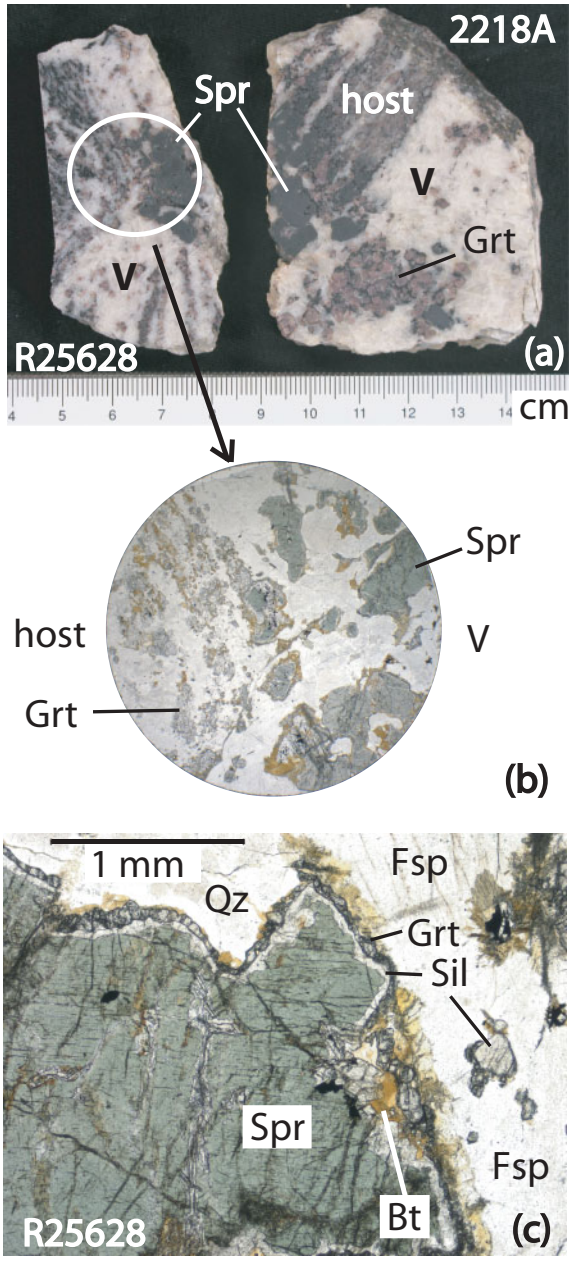

Fig. 3. Host quartz-rich paragneisses and interboudin pockets from McIntyre Island. (a) Rock slabs with aggregates of coarse sapphirine crystals in boudin neck in sample R25628 and adjacent to boudin of paragneiss host in interboudin pocket (V) in sample 2218A. (b) Photomicrograph of section (diameter 2·5 cm) of boudin neck in sample R25628; plane-polarized light. (c) Photomicrograph of sample R25628 showing coarse sapphirine with corona of sillimanite and garnet in the interboudin pocket; plane-polarized light. Biotite (Bt, brown) not only overgrows the corona, but also is found along fractures cutting sapphirine. Fsp, highly perthitic feldspar.

metamorphism (e.g. White & Powell, 2002), but textural relations are rather equivocal (e.g. Fig. 4a). Cordierite is present in only a few sections, and appears to a late-formed phase.

In the quartz-rich paragneisses at Christmas Point, coronae of secondary sillimanite and orthopyroxene or garnet separate sapphirine and quartz (e.g. Sandiford, 1985; Grew *et al.*, 2000); direct contact of sapphirine with quartz is rare (Fig. 4a). Orthopyroxene and garnet also form independent grains that are presumed to be primary; e.g. orthopyroxene grains up to 3·5 mm containing oriented needles of rutile. A trace of cordierite occurs in a band along a fracture in one sapphirine-free sample (2292H) and in seams with fine-grained orthopyroxene cutting garnet in one sapphirine-bearing sample (2292J).

The host-rocks from Zircon Point differ in that orthopyroxene is absent and garnet widespread in sillimanite-bearing rocks: in places garnet forms pods 1–2 cm thick. Samples 2234A and 2234B contain pods up to 2 cm across of calcic plagioclase. These are blue–green in hand specimen as a result of abundant, disseminated, fine-grained spinel that is commonly overgrown by sillimanite. A few grains of sapphirine, some cored by spinel, and corundum are also present. Sapphirine forms tiny grains enclosed in garnet porphyroblasts in 2234B and 2234E. Samples 2234E and R31050 contain a distinctive suite of accessory phases, e.g. perrierite/chevkinite in 2234E; niobian rutile, an unidentified phase containing rare earth elements and U, and huttonite–monazite in R31050.

Paragneisses from Mount Pardoe have two generations of orthopyroxene, garnet and sillimanite that are distinguished by marked difference in size and the presence of abundant acicular rutile inclusions in primary orthopyroxene. Cordierite occurs with sillimanite or sillimanite + orthopyroxene intergrowths in samples 10507 and 10513, and is interpreted to be a secondary phase formed by reaction of sillimanite with orthopyroxene. Sapphirine is relatively sparse and is invariably enclosed in sillimanite or is surrounded by sillimanite corona (Fig. 4b). Foliation is well developed in several samples as a result of the shape of very fine-grained aggregates of sillimanite + orthopyroxene or of clusters of coarse orthopyroxene.

Boudins at McIntyre Island are garnet–sillimanite paragneisses (Fig. 3a and b). Sapphirine occurs sparingly as medium-sized grains mantled by sillimanite with corundum; an outer garnet corona is locally present. Rare spinel and sapphirine are enclosed in sillimanite prisms. Sample 2218A is unique among the samples studied in that garnet is mantled by successive coronae of cordierite and orthopyroxene.

Anatectic pods, veins and interboudin pockets

The beryllium pods at Christmas Point are zoned with a quartz core surrounded by an outer zone rich in red microcline (Grew, 1981, 1998; Grew *et al.*, 2000). Sillimanite in prisms up to 10 cm long and 4 cm across is

Table 1: Minerals in the quartz-rich paragneisses and veins

Locality:	Christmas Pt.	Zircon Pt.	Mt. Pardoe	Mt. Pardoe	McIntyre I.	McIntyre I.
Rock type:	P	P	P	V	P	V
n (specimens):	11	7	7	1	3	3
n (whole-rock analyses):	11	6	8	1	2	0
Quartz (Qtz, Qz, Q)	X	X	X	X	X	X
Alkali feldspar (Kfs)	X	X	X*	X*	X*	X*
Plagioclase (Pl)	T	X	X*	X*	X*	X*
Sillimanite (Sil)	X	X	X	X	X	X
Kyanite	—	—	—	T	—	—
Andalusite	—	—	—	T	—	—
Orthopyroxene (Opx)	X	—	X	X	T	T
Sapphirine (Spr)	X	T	T	—	T	X
Garnet (Grt)	X	X	X	X	X	X
Biotite (Bt)	X	X	X	X	X	X
Muscovite	T	T	—	T†	—	—
Chlorite	T	T	T	T†	—	—
Cordierite (Crd)	T	—	T	X	T	T
Zircon (Zrn)	A	A	A	A	A	A
Perrierite/chevkinite	—	T	—	—	—	—
Corundum (Crn)	A	T	—	—	T	T
Spinel (Spl)	—	T	—	—	T	T
Rutile (Rt)	A	A	A	A	A	A
Niobian rutile	—	T	—	—	T	—
Davidite-(Ce)	T	—	—	—	—	—
REE—Ti unknown	—	T	—	—	—	—
U-rich unknowns	—	T	—	T	—	T
Apatite group	—	T	—	T‡	—	T
Wagnerite	—	—	—	T	—	—
Monazite (Mnz)	A	T	A	A	A	A
Huttonite	—	T	T	—	—	—
Xenotime	T	—	—	A	—	—
Carbonate	—	—	—	—	—	T

Only minerals found in the analyzed (whole-rock, microprobe) samples are listed here; Grew *et al*. (2000, table 1) gave a complete listing for Christmas Point and Mount Pardoe. P, quartz-rich paragneiss; V, vein or interboudin pocket. ×, present in most samples or abundant; T, present in relatively few sections and never abundant; A, accessory phase present in most samples. The abbreviations given in parentheses have been used throughout the paper.
*In large part components of microperthite.
†Presumed to be a component of pinite replacing cordierite.
‡Chlorapatite (Roy *et al.*, 2003).

found in both zones (e.g. Fig. 2b), whereas the Be minerals are largely found in the quartz cores. Beryllian sapphirine and khmaralite form deeply embayed masses up to 5 cm across that are surrounded by an inner corona of medium-grained sillimanite and an outer corona of granular garnet with minor quartz; nowhere are sapphirine and khmaralite in contact with quartz. Overall, most of the Be is concentrated in surinamite–sillimanite–garnet ± orthopyroxene–quartz aggregates that resulted from the complete replacement of sapphirine–khmaralite. Moats of cordierite separate garnet, surinamite and sillimanite within the surinamite-bearing aggregates. Textures suggest that orthopyroxene is coeval with surinamite, sillimanite and garnet in some cases (Grew, 1998), but later in others (Grew *et al.*, 2000); orthopyroxene included in a coarse sillimanite prism (sample 12218) belongs to an earlier generation. The only likely primary biotite forms flakes up to 2 cm thick (e.g. sample

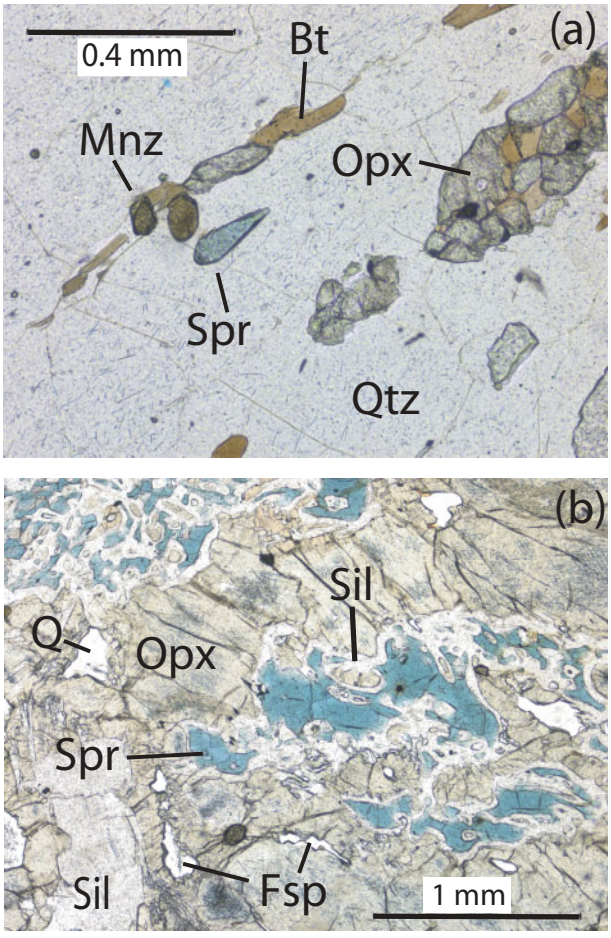

Fig. 4. Photomicrographs in plane-polarized light. (a) Sample 2292M (Christmas Point) showing sapphirine containing 2100 ppm Be in direct contact with quartz. Mnz, monazite (modified from Grew *et al.*, 2000). (b) Sample 10503 (Mount Pardoe) showing sapphirine containing 30 ppm Be separated by sillimanite from contact with orthopyroxene containing fine acicular rutile. Fsp, unspecified feldspar.

12269); the finer-grained, more abundant variety is undoubtedly secondary (Grew *et al.*, 2000).

Sample R25518 is a coarse-grained sapphirine–sillimanite segregation at Christmas Point. It contains traces of wagnerite and fluorapatite, which suggest an affinity with the anatectic pods in which these phosphates are common; neither phosphate has been found in the paragneisses at this locality.

Be mineral associations in the Zircon Point Be pod are similar to those in the Christmas Point pods except for the presence of boron, which is manifested in dumortierite and 150–500 ppm B in khmaralite, sillimanite and surinamite (Grew, 1981, 1998, 2000*b*; Barbier *et al.*, 1999; Grew *et al.*, 2000). Indeed, no other Late Archean anatectic rock in the Napier Complex manifests boron.

The Mount Pardoe Be veins are unzoned (Fig. 2c) and consist of cream-colored mesoperthitic feldspar and quartz; early-formed accessory minerals include orthopyroxene up to 2 cm across, garnet and wagnerite (Grew *et al.*, 2000; Roy *et al.*, 2003). Zircon is relatively rare. Surinamite occurs in trace amounts enclosed in cordierite with sillimanite, garnet and biotite in sample 10510. Cordierite is also found around garnet and near orthopyroxene in several samples, including 10514.

Anatectic veins filling the spaces between boudins from McIntyre Island (Table 1) locally contain primary coarse anhedral to subhedral sapphirine grains (Fig. 3a and b); these grains enclose lamellae of garnet or orthopyroxene. Sapphirine is invariably separated from quartz and mesoperthite by an inner corona of sillimanite and an outer corona of garnet or, less commonly, orthopyroxene. Corundum and spinel are found partially enclosed in sapphirine or between sillimanite and sapphirine; both appear to have resulted from sapphirine breakdown. Cordierite occurs locally around medium-grained garnet. Biotite is typically developed as an irregular, discontinuous outermost corona around sapphirine and garnet (Fig. 3c).

Textures suggest that the anatectic veins at the four localities had a three-stage evolution as follows.

(1) Sapphirine crystallized together with quartz and K-feldspar in the presence of melt [Christy *et al.* (2002) attributed the superstructure characteristic of khmaralite to later annealing of beryllian sapphirine with $\geq$0·5 Be/20 O]. Conventional U–Pb data gave 2450–2500 Ma for crystallization of the vein (Grew 1998), but new sensitive high-resolution ion microprobe (SHRIMP) data give 2590–2550 Ma on similar anatectic veins from McIntyre Island (Harley, 2004). Discordant relationships with the hosting paragneisses imply that the veins were emplaced after the peak of deformation and UHT metamorphism, but probably still at very high temperatures where sapphirine could form by reactions involving melt.

(2) Under granulite-facies conditions sapphirine reacted with quartz to form successive coronae of sillimanite and garnet. At Christmas Point and Zircon Point coronae developed from beryllian sapphirine contain surinamite and other Be minerals. Except for rare surinamite, no trace of the coronae remains in the Mount Pardoe vein. This stage has not been dated. It could be coeval with sillimanite–orthopyroxene–garnet coronae in the paragneisses that are attributed by most investigators to isobaric cooling following the UHT metamorphic peak (e.g. Sheraton *et al.*, 1987; Harley, 2004).

(3) Under lower-temperature conditions, largely in the amphibolite facies, andalusite, kyanite, cordierite, orthoamphibole and most biotite formed. This stage is related either to Late Proterozoic ('Rayner') or Early Paleozoic ('Pan-African') activity reported in Casey and Amundsen Bays (Black *et al.*, 1983; Sandiford & Wilson, 1984; Harley, 1985; Carson *et al.*, 2002).

MINERAL COMPOSITION

Constituents with $Z > 8$

Detailed analytical procedures are reported in Electronic Appendix 1, available on the *Journal of Petrology* web site at http://www.petrology.oxfordjournals.org.

Orthopyroxene and garnet

Overall, the complex textural relationships among the minerals in the quartz-rich paragneisses and associated veins result in complicated interpretations of the compositional relationships, most notably among the three textural varieties of orthopyroxene and garnet: (1) cores of the relatively large grains; (2) rims of the relatively large grains; (3) coronae and small grains formed by reaction of sapphirine with quartz (i.e. secondary orthopyroxene and garnet). In addition, the composition varies from grain to grain for a given mineral texture in some thin sections.

Orthopyroxene is aluminous and zoned (Table 2 and Electronic Appendix 2, available for downloading at http://www.petrology.oxfordjournals.org), features characteristic of orthopyroxene in granulites elsewhere in the Napier Complex (e.g. Harley & Motoyoshi, 2000). Compositions determined along traverses across large grains in granulites from Christmas Point (2292F, 2292J and 2292M) and Mount Pardoe (10501, 10503, 10504) show that cores are richer in Al and poorer in Si and Mg than rims, whereas zoning in Fe and Ca is much less marked. These relationships imply that the Tschermaks exchange largely involves Mg, and little or no Fe, i.e. $MgSiAl_{-2}$. The Al_2O_3 contents of orthopyroxene decrease in the order core > rim > corona in some cases (e.g. sample R31238), but more commonly the Al_2O_3 contents of rims and coronae overlap. In samples where X_{Mg} [= Mg/(Mg + Fe)] of orthopyroxene varies over a narrow range, it increases slightly with decreasing Al (e.g. R31238, 2292M, Table 2), but in other samples there is significant grain-to-grain variation in X_{Mg}.

Garnet is typically an almandine–pyrope solid solution with 40–60 mol % pyrope and no more than 7 mol % of spessartine + grossular + YAG ($Y_3Al_5O_{12}$) (Table 2 and Electronic Appendix 3, available for downloading at http://www.petrology.oxfordjournals.org). The YAG component ranges from below detection to 1 mol %, and typically decreases in the order core > rim > corona. Traverses across large grains in paragneisses from Christmas Point (2292F, 2292G), Mount Pardoe (10504) and Zircon Point (2234E) show little zoning in Mg, Fe and Mn, whereas zoning in Ca and Y is variable; in some samples these constituents are markedly enriched in the core. In contrast to orthopyroxene, X_{Mg} is markedly lower in coronal garnet compared with the coarse-grained garnet in samples from Christmas Point (e.g. Table 2).

Feldspars

Analyses of potassic and sodic feldspar are relatively few because feldspar is commonly too perthitic or antiperthitic to obtain meaningful spot analyses; tabulated analyses are typically hosts (Table 2 and Electronic Appendix 4, available for downloading at http://www.petrology.oxfordjournals.org). Plagioclase is oligoclase in paragneisses from Mount Pardoe (An18–20), andesine in a paragneiss from Christmas Point (An32–33), and labradorite in the blue–green pods in the Zircon Point paragneisses (An53–66).

Sapphirine and sillimanite

Sapphirine compositions are close to the 7:9:3 composition, $(Mg,Fe^{2+})_{3.5}(Al,Fe^{3+},Cr,V)_9Si_{1.5}O_{20}$, or are more siliceous, but incorporation of Be results in a further increase of Si (see below). Cr and V contents are measurable only in paragneisses and associated interboudin pockets from McIntyre Island, i.e. Cr_2O_3 up to 1·3 wt % and 0·5 wt %, and V_2O_3 up to 0·4 and 0·2 wt % in sapphirine (Table 3) and sillimanite, respectively (Table 2 and Electronic Appendix 5, available for downloading at http://www.petrology.oxfordjournals.org).

Biotite

Biotite in the paragneisses is characterized by relatively high F (1·4–6·2 wt %) and TiO_2 (2·4–4·1 wt %), but negligible Cl; (Si + Al) ≈ 8 (i.e. $^{vi}Al \approx 0$) per 20 O + 4 (OH,F,Cl); in only a few analyses does (Si + Al) reach 8·2 (Table 4). Biotite in the veins contains significant Cl (+ and × in Fig. 5). In terms of Ti content and X_{Mg} = Mg/(Mg + Fe), the compositions of biotite from Napier Complex paragneisses (except the nearly end-member F-dominant phlogopite from Mount Riiser-Larsen; Motoyoshi & Hensen, 2001) and veins (except those from Christmas Point) plot near or above the 800°C isotherm for biotite from rocks saturated in SiO_2 and TiO_2 (Henry *et al.*, 2005). However, there is not a good correspondence between temperatures indicated by the isotherms and relative time of formation inferred from textures. A secondary origin is clearly indicated for most biotite in the veins (e.g. Fig. 3c); an exception is coarse-grained, presumably primary biotite in pod sample 12269, which plots at a lower temperature. Motoyoshi & Hensen (2001) inferred a high-temperature origin for F-dominant phlogopite with F/(F + OH) >0·75, yet these plot at lower temperatures than clearly secondary biotite (e.g. Osanai *et al.*, 2001) and biotite that might be secondary (e.g. Fig. 4a). These anomalies suggest that both Cl and F affect Fe–Mg–Ti relationships in biotite and that the isotherms cannot be applied to biotite varying widely in halogen content.

Table 2: Summary of selected chemical data on major rock-forming minerals

	Orthopyroxene													
Sample:	C. Pt. R31238	C. Pt. R31238	C. Pt. R31238	C. Pt. 2292J	C. Pt. 2292J	C. Pt. 2292M	C. Pt. 2292M	C. Pt. 2292M	Mt. P. CC6	Mt P. 10503	Mt. P. 10503	Mt. P. 10504	Mt. P. 10504	Mc. I. R25628*
Texture:	core	rim	2nd	core	2nd	core	rim	2nd	core	core	2nd	core	rim	2nd
Be ppm	15·3	13·5	9·2	9·2	7·9	14·0	12·4	9·6	1·7	—	0·1	—	—	0·4
Al/6 O	0·323	0·286	0·252	0·343	0·286	0·322	0·260	0·261	0·306	0·407	0·277	0·458	0·278	0·334
X_{Mg}	0·826	0·830	0·830	0·770	0·758	0·818	0·823	0·824	0·774	0·742	0·756	0·752	0·765	0·704

	Garnet													
Sample:	C. Pt. 2292F	C. Pt. 2292F	C. Pt. 2292F	C. Pt. 2292J	C. Pt. 2292J	C. Pt. 2292J	Z. Pt. 2234A1	Z. Pt. 2234A3	Z. Pt. 2234E	Mt. P. 10504	Mt. P. 10504	Mt. P. 10504	Mc. I R25628	Mc. I R25628*
Texture:	core	rim	2nd	core	rim	2nd	core	core	core	core	rim	2nd	core	2nd
Be ppm	—	—	—	—	—	—	0·05	0·06	0·6	—	—	—	—	0·2
Alm	0·379	0·377	0·447	0·378	0·373	0·479	0·460	0·434	0·426	0·388	0·388	0·387	0·525	0·529
Prp	0·582	0·585	0·519	0·587	0·592	0·482	0·488	0·504	0·554	0·577	0·580	0·583	0·449	0·450
Sps	0·002	0·002	0·000	0·004	0·003	0·006	0·006	0·006	0·004	0·014	0·015	0·015	0·006	0·005
Grs	0·034	0·034	0·033	0·022	0·024	0·031	0·043	0·056	0·006	0·013	0·012	0·012	0·018	0·015
YAG	0·003	0·001	0·000	0·010	0·008	0·003	0·003	0·001	0·010	0·008	0·005	0·004	0·003	0·000

	Feldspar											
Sample:	C. Pt. R31238	C. Pt. 2292L	C. Pt. 2292L	Z. Pt. 2234A1	Z. Pt. 2234A3	Z. Pt 2234B	Z. Pt. 2234E	Mt. P. CC6	Mt. P. 10503	Mt. P. 10503	Mt. P. 10514*	Mt. P. 10514*
Be ppm	—	0·2	11	0·3	19	42	0·2	0·6	—	—	0·5	6·0
Ab	11·4	10·9	66·5	12·2	39·5	44·0	7·5	78·4	11·1	84·8	6·8	82·5
An	0·2	0·2	32·7	0·7	59·6	55·1	0	19·2	0·1	14·5	0·2	16·8
Or	87·0	86·0	0·8	87·0	0·8	0·9	92·5	2·4	87·5	0·6	92·6	0·7
Cn	1·5	2·9	0	0·2	0	0	0	0	1·3	0	0·4	0

	Sillimanite												
Sample:	C. Pt. R31238	C. Pt. 2292F	C. Pt. 2292J	C. Pt. 2292M	C. Pt. 12263*	Z. Pt. 2234A1	Z. Pt. 2234A3	Z. Pt. 2234E	Mt. P. CC6	Mt. P. 10503	Mc. I R25628	Mc. I R25628*	Mc.I. 2218A*
Be ppm	8·6	3·7	6·8	12	37	7·3	5·7	22	1·2	0·1	6·0	3·3	1·4
V/5 O	0	0·001	0·001	0·001	0	0	0·002	0	0	0	0·002	0·003	0·003
Cr/5 O	0	0	0	0	0	0	0·002	0	0	0	0·010	0·007	0·006
Fe/5 O	0·009	0·017	0·014	0·010	0·026	0·005	0·005	0·007	0·009	0·009	0·005	0·006	0·007

Localities: C. Pt., Christmas Point; Z. Pt., Zircon Point; Mt. P., Mount Pardoe; Mc. I., McIntyre Island. Samples are paragneisses unless indicated by * for pod, vein or interboudin pocket. Values are mole proportions or formula units for the oxygens specified. Alm, almandine; Prp, pyrope; Sps, spessartine; Grs, grossular; YAG, $Y_3Al_5O_{12}$; Ab, albite; An, anorthite; Or, orthoclase; Cn, celsian. For full analyses, see Electronic Appendices 2–5, available for downloading at http://www.petrology.oxfordjournals.org.

Table 3: Selected analyses of sapphirine

Locality:	C. Pt.	C. Pt.	C. Pt.	C. Pt.	Z. Pt.	Z. Pt.	Z. Pt.	Mt. P.	Mt. P.	Mc. I.	Mc. I.	Mc. I.	Mc. I.
Rock type:	P	P	P	P	P	P	P	P	P	P	V	V	V
Sample:	R31238	2292F*	2292J	2292M	2234A3	2234B*	2234E	CC6	10503	R25628	R25628	2218A*	2223J*
wt %													
SiO_2	13·67	13·18	13·49	14·52	13·49	15·02	15·51	13·45	13·79	13·52	13·76	14·05	13·96
TiO_2	0	0·12	0·04	0·07	0·04	0·05	0·06	0	0	0·04	0·05	0·06	0·04
Al_2O_3	62·46	60·67	61·15	61·09	62·57	60·70	59·16	62·05	61·00	61·05	59·83	59·42	60·21
V_2O_3	0	0·03	0·06	0	0·09	0·03	0	0·01	0	0·16	0·35	0·31	0·19
Cr_2O_3	0	0	0·02	0	0·17	0·05	0	0	0	1·22	0·71	0·68	0·49
Fe_2O_3	2·61	3·84	3·12	2·16	1·21	1·28	2·36	2·13	1·82	2·30	2·22	1·31	1·37
FeO	2·43	4·90	4·32	3·27	4·76	5·64	4·49	4·40	5·70	4·72	5·91	6·59	5·84
MnO	0	0	0	0·05	0·02	0	0	0·04	0·06	0·08	0·06	0	0·03
MgO	18·59	17·05	17·44	18·38	17·24	16·96	17·82	17·76	17·25	16·97	16·92	16·64	17·10
CaO	0·02	0	0·01	0	0·05	0·04	0	0·07	0	0·02	0	0·01	0·01
Na_2O	0	0	0	0	0·01	0	0	—	0·01	0·01	0	0	0·01
BeO	0·42	0·21	0·31	0·63	0·27	0·86	0·95	0·02	0·01	0·43	0·10	0·09	0·05
Sum	100·19	100·01	99·97	100·16	99·93	100·64	100·36	99·95	99·64	100·53	99·92	99·19	99·31
ppm													
Li	32	36	48	—	32	36	22	43	—	52	60	104	84
Be	1514	754	1107	2277	984	3086	3429	58	34	1566	369	335	184
B	0·5	0·1	0·3	—	23	10	0·4	1·5	—	2·5	0·5	2·3	1·7
Formulae per 14 cations/20 oxygens													
Si	1·595	1·567	1·596	1·695	1·589	1·756	1·814	1·588	1·641	1·593	1·642	1·687	1·668
Ti	0	0·011	0·003	0·006	0·003	0·005	0·005	0	0	0·004	0·004	0·005	0·003
Al	8·585	8·502	8·521	8·408	8·687	8·363	8·157	8·637	8·557	8·482	8·413	8·412	8·481
V	0	0·003	0·006	0	0·009	0·003	0	0·001	0	0·015	0·034	0·030	0·018
Cr	0	0	0·002	0	0·016	0·004	0	0	0	0·114	0·067	0·065	0·046
Fe^{3+}	0·229	0·344	0·278	0·190	0·108	0·113	0·208	0·190	0·163	0·204	0·199	0·118	0·123
Fe^{2+}	0·237	0·488	0·427	0·320	0·469	0·551	0·439	0·435	0·567	0·465	0·590	0·662	0·584
Mn	0	0	0	0·005	0·002	0	0	0·004	0·006	0·008	0·006	0	0·003
Mg	3·232	3·023	3·073	3·200	3·028	2·956	3·107	3·126	3·061	2·982	3·009	2·980	3·046
Ca	0·002	0	0·002	0	0·006	0·005	0	0·009	0	0·002	0	0·002	0·001
Na	0	0	0	0	0·002	0	0	—	0·002	0·003	0	0	0·003
Li	0·003	0·004	0·005	—	0·003	0·004	0·002	0·004	—	0·005	0·006	0·011	0·009
Be	0·118	0·060	0·087	0·177	0·077	0·241	0·267	0·005	0·003	0·123	0·029	0·027	0·015
Sum	14	14	14	14	14	14	14	14	14	14	14	14	14
X_{Mg}	0·932	0·861	0·878	0·909	0·866	0·843	0·876	0·878	0·843	0·865	0·836	0·818	0·839

Localities: C. Pt., Christmas Point; Z. Pt., Zircon Point; Mt. P., Mount Pardoe; Mc. I., McIntyre Island. P, paragneiss; V, interboudin pocket. Sums include wt % Li_2O. Fe^{2+} and Fe^{3+} calculated from stoichiometry. X_{Mg} = atom Mg/(Mg + Fe^{2+}). K_2O is 0–0·02 wt %.
*Data on Li, Be and B are averages for several grains in the sample.

Oxides

Green spinel in Zircon Point paragneisses contains 18–23 mol % gahnite (9–11 wt % ZnO), but Cr_2O_3 ≤0·5 wt %, whereas brown spinel in McIntyre Island interboudin pockets contains up to 8·1 wt % Cr_2O_3 and 0·6 wt % V_2O_3 (see Electronic Appendix 6, available for downloading at http://www.petrology.oxfordjournals.org). Nb and Ta contents of rutile are locally significant, reaching a maximum of 25 wt % Nb_2O_5 and 2·8 wt % Ta_2O_5 in samples R31050 and R25628, respectively.

Table 4: Selected analyses of biotite

Locality:	C. Pt.	C. Pt.	C. Pt.	C. Pt.	C. Pt.	Z. Pt.	Z. Pt.	Mt. P.	Mt. P.	Mt. P.	Mc. I.	Mc. I.	Mc. I.	Mc. I.
Rock:	P	P	P	P	V	P	P	P	P	V	P	V	V	V
Sample:	R31238	R31243	2292G	2292M	12216	2234A1	2234E	CC6	10503	10514	R25628	R25628	2218A	2223J
wt %														
SiO_2	38·87	37·29	38·79	38·65	38·37	39·60	41·87	39·32	40·19	39·10	38·42	38·48	36·92	39·94
TiO_2	3·98	3·77	2·55	4·08	0·83	3·10	2·46	3·39	4·14	3·64	3·76	3·90	4·38	4·79
Al_2O_3	14·45	15·87	15·39	14·61	16·20	14·35	13·17	14·20	14·05	13·84	14·45	14·39	16·27	13·07
Cr_2O_3	0	0·01	0	0·01	0	0	0	0	0	0·01	0·10	0·15	0·29	0·13
FeO	4·51	8·57	5·98	5·36	10·22	5·36	3·36	5·05	6·25	8·24	7·13	7·37	8·62	7·76
MnO	0	0·01	0	0	0	0·01	0	0·01	0·02	0·02	0	0	0	0
MgO	22·78	19·15	22·32	22·03	19·75	22·57	24·92	23·25	21·46	20·31	20·85	20·51	18·24	19·95
CaO	0	0	0	0	0	0·01	0	0	0	0	0	0	0·03	0·02
Na_2O	0·13	0·13	0·57	0·15	0·15	0·10	0·14	0·32	0·17	0·10	0·12	0·13	0·14	0·15
K_2O	10·17	9·71	8·84	10·04	9·62	10·35	10·50	10·07	10·09	9·82	10·01	10·01	9·70	9·58
BaO	0·41	0·88	0·88	0·66	0	0·05	0	0·11	0·11	0	0·21	0·33	0·24	0
F	2·78	1·48	2·15	2·84	1·48	3·18	5·96	3·50	3·35	2·65	2·93	2·95	0·87	2·70
Cl	0·03	0·02	0	0·04	0·58	0·02	0·02	0	0·02	0·79	0·09	0·06	0·32	0·77
H_2O	2·87	3·40	3·17	2·82	3·26	2·69	1·46	2·55	2·64	2·68	2·72	2·72	3·61	2·69
O = F,Cl	−1·17	−0·63	−0·90	−1·21	−0·75	−1·34	−2·52	−1·48	−1·42	−1·30	−1·26	−1·26	−0·44	−1·31
Sum	99·81	99·66	99·73	100·08	99·72	100·04	101·35	100·30	101·08	99·90	99·54	99·77	99·19	100·25
ppm														
Be	3·1	—	7·0	3·2	4·0	0·7	0·7	0·06	—	0·6	1·4	1·3	—	—
Formulae per 20 O + 4(OH,F,Cl)														
Si	5·560	5·444	5·561	5·543	5·594	5·653	5·848	5·598	5·693	5·671	5·568	5·575	5·402	5·748
^{iv}Al	2·436	2·556	2·439	2·457	2·406	2·347	2·152	2·384	2·307	2·329	2·432	2·425	2·598	2·217
Sum iv	7·996	8	8	8	8	8	8	7·982	8	8	8	8	8	7·965
Ti	0·429	0·414	0·275	0·441	0·091	0·332	0·258	0·363	0·441	0·397	0·410	0·425	0·482	0·519
^{vi}Al	0	0·174	0·163	0·012	0·378	0·068	0·016	0	0·037	0·036	0·037	0·033	0·207	0
Cr	0	0·001	0	0·001	0	0	0	0	0	0·002	0·011	0·017	0·033	0·015
Fe	0·540	1·046	0·717	0·643	1·247	0·640	0·393	0·602	0·740	1·000	0·864	0·893	1·054	0·934
Mn	0	0·001	0	0	0	0·002	0	0·002	0·003	0·003	0	0	0	0
Mg	4·859	4·166	4·772	4·710	4·292	4·804	5·188	4·936	4·531	4·390	4·505	4·429	3·978	4·280
Sum vi	5·827	5·803	5·926	5·806	6·008	5·846	5·855	5·902	5·753	5·827	5·827	5·798	5·754	5·748
Na	0·037	0·038	0·158	0·041	0·041	0·029	0·038	0·088	0·047	0·027	0·035	0·038	0·040	0·043
K	1·855	1·807	1·617	1·837	1·790	1·885	1·871	1·829	1·822	1·816	1·851	1·851	1·811	1·759
Ca	0	0	0	0	0	0·001	0	0	0	0	0	0	0·004	0·003
Ba	0·023	0·050	0·049	0·037	0	0·003	0	0·006	0·006	0	0·012	0·019	0·014	0
Sum xii	1·915	1·896	1·825	1·915	1·831	1·918	1·910	1·923	1·876	1·844	1·898	1·908	1·870	1·805
Sum cations	15·739	15·699	15·751	15·720	15·839	15·764	15·765	15·806	15·629	15·671	15·725	15·706	15·623	15·518
F	1·256	0·684	0·973	1·290	0·682	1·435	2·634	1·578	1·502	1·217	1·345	1·352	0·401	1·227
Cl	0·006	0·004	0	0·010	0·143	0·005	0·005	0	0·004	0·195	0·023	0·016	0·080	0·187
OH	2·738	3·312	3·027	2·700	3·175	2·559	1·362	2·422	2·494	2·589	2·632	2·632	3·519	2·586
Sum	4	4	4	4	4	4	4	4	4	4	4	4	4	4
X_{Mg}	0·900	0·799	0·869	0·880	0·775	0·882	0·930	0·891	0·860	0·815	0·839	0·832	0·791	0·821

Localities: C. Pt., Christmas Point; Z. Pt., Zircon Point; Mt. P., Mount Pardoe; Mc. I., McIntyre Island. P, paragneiss; V, pod, vein or interboudin pocket. All Fe as FeO. H_2O was calculated assuming (OH + F + Cl) = 4.

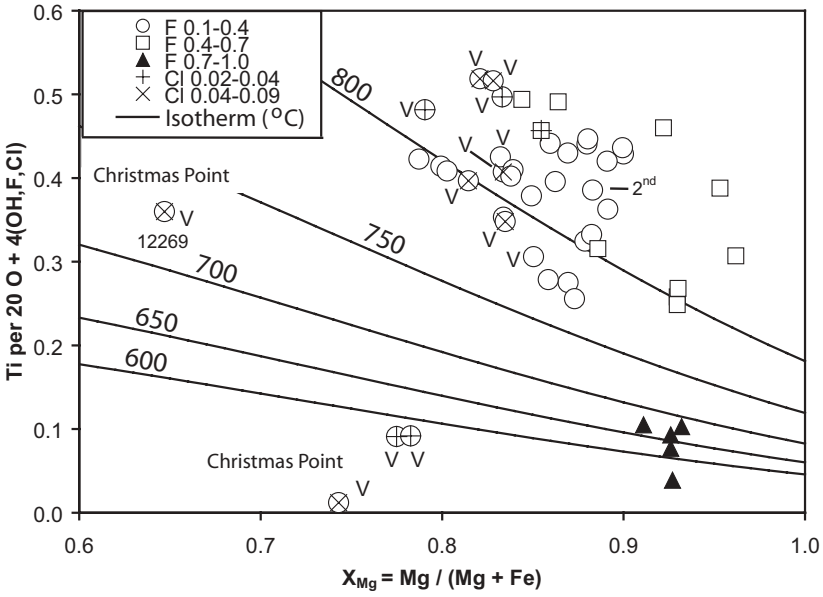

Fig. 5. X_{Mg}, Ti and halogen contents of biotite, including data from Casey Bay and Mount Pardoe (Table 4; Grew *et al.*, 2000), Bunt Island in Amundsen Bay (Osanai *et al.*, 2001, marked '2nd'), and the Tula Mountains (Grew, 1980, 1982; Motoyoshi & Hensen, 2001). Isotherms (°C) are from Henry *et al.* (2005). Legend refers to $X_F = F/(F + Cl + OH)$ and $X_{Cl} = Cl/(F + Cl + OH)$. V, biotite from veins, pods and interboudin pockets.

The composition of a davidite-(Ce) grain between rutile and zircon in sample R31243 is $Mg_{0.4}Ca_{0.1}Fe^{2+}_{3.5}Pb_{0.1}Al_{1.3}Fe^{3+}_{2.0}Y_{0.2}La_{0.3}Ce_{0.5}Ti_{13.2}Zr_{0.3}Th_{0.1}U_{0.2}O_{38}$.

Distribution of components among the phases

Mg–Fe^{2+} partitioning decreases in the order sapphirine ≈ biotite > orthopyroxene > garnet and is more regular between sapphirine and orthopyroxene or biotite than between sapphirine and garnet (Fig. 6a). Ferromagnesian silicates are on average less magnesian in the veins than in the paragneisses hosting the veins at a given locality. Fe^{3+} calculated for sapphirine increases with sillimanite Fe^{3+} (Fig. 6b). Christmas Point paragneisses and pods are more oxidized than those from the other three localities. Random error in calculating the sapphirine Fe^{3+}/Fe^{2+} ratio from stoichiometry probably contributes to scatter in the data, whereas paucity of Fe^{3+}-rich samples or systematic errors could be responsible for the non-zero intercept in Fig. 6b. None the less, the distribution of Fe^{2+}, Fe^{3+} and Mg evident in Fig. 6 is fairly regular as is Be distribution (see below), which is consistent with an approach to chemical equilibrium during metamorphism.

Boron and lithium

Boron contents are ≤0·2 ppm in two analyzed samples of orthopyroxene and 0·1–0·7 ppm in quartz. B contents in sillimanite generally range from <0·1 to 3 ppm; contamination is suspected in measurements giving 7–16 ppm B on three prisms in samples where other prisms give much lower values. B contents in sapphrine generally range from <0·1 to 4 ppm, with the exception of 5–23 ppm B in sapphirine grains 0·05–0·15 mm across included in plagioclase in samples 2234A and 2234B from Zircon Point.

Lithium contents are negligible in the one sillimanite analyzed (~0·1 ppm Li, sample 10504), but lithium is more abundant in quartz (~0·1–2 ppm Li) and orthopyroxene (7–8 and 15 ppm Li in samples 2292F and 10504, respectively). Sapphirine contains 21–113 ppm Li, which increases regularly with the whole-rock Li content, whereas the ratio of Li in sapphirine to whole-rock Li content decreases from 7·4 to 2·4 (Fig. 7). Sapphirine is, thus, a major carrier of Li, particularly at low whole-rock Li concentrations. It is not the only mineral to concentrate Li, because biotite, for which Li was not determined in this study, has been shown to concentrate Li in high-grade rocks elsewhere (e.g. Shaw *et al.*, 1988), probably to a similar extent as sapphirine (Grew *et al.*, 1990).

Beryllium

Be contents of individual grains of sapphirine range from 25 to 3430 ppm, corresponding to 0·002–0·267 Be per 14 cations/20 oxygen (e.g. Fig. 8). Be increases concomitantly with Si in a roughly 1:1 ratio for all the samples considered together and for individual grains in many samples, consistent with the substitution $BeSiAl_{-2}$, which is characteristic of beryllian sapphirine and khmaralite (Barbier *et al.*, 1999; Grew *et al.*, 2000; Christy *et al.*, 2002; Grew, 2002*b*). Si variation exceeds Be variation in

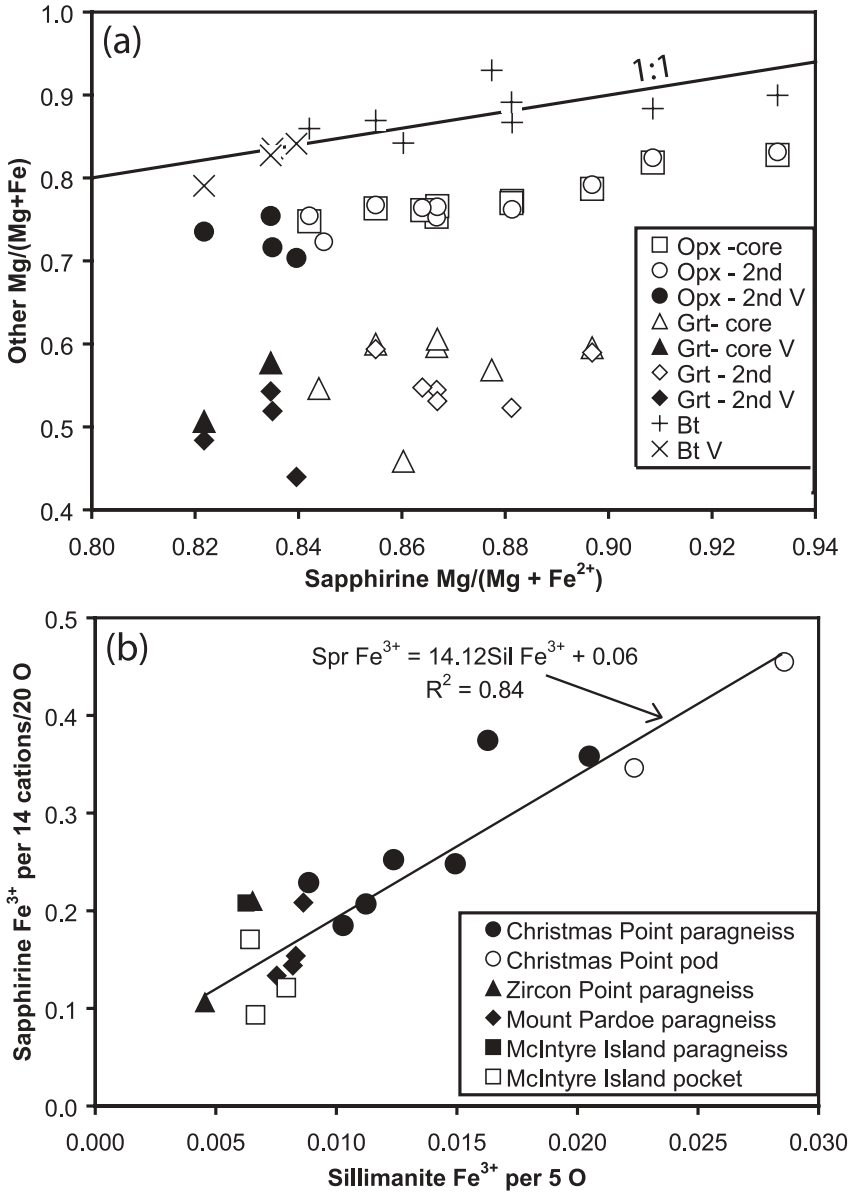

Fig. 6. Distribution of Fe and Mg among the major rock-forming minerals. (a) Average mole fraction Mg/(Mg + Fe) of associated sapphirine, orthopyroxene, garnet and biotite for paragneisses and anatectic pods, veins and interboudin pockets (V suffix) from all four localities. Fe is the measured Fe for all minerals except sapphirine, whose Fe^{2+} content was calculated from stoichiometry. '2^{nd}' (secondary) refers to (1) coronae and small grains of orthopyroxene and garnet formed by reaction of sapphirine with quartz, and (2) small grains of orthopyroxene and garnet next to orthopyroxene and garnet in much coarser grains; also garnet coronae around orthopyroxene and sillimanite. Reference line marked 1:1 indicates equal distribution. (b) Fe^{3+} contents of associated sapphirine and sillimanite. Fe^{3+} is total Fe in sillimanite; sapphirine Fe^{3+} content was calculated from stoichiometry. Line is least-squares fit to all the data; equation is based on this line. Christmas Point pods include samples R25518 and 12263.

sapphirine with <0·05 Be per 20 oxygens and in sample 2292M, i.e. the Tschermaks substitution $MgSiAl_{-2}$ is dominant in these samples.

Be contents of cordierite range from 560 to 930 ppm in a paragneiss (10513) and from 360 to 2600 ppm in two veins (e.g. see Electronic Appendix 7, available for downloading at http://www.petrology.oxfordjournals.org). Incorporation of Be closely fits the substitution $Be(Na,K)Al_{-1}\square_{-1}$, which is characteristic of natural cordierite (e.g. Grew, 2002*b*), with a small contribution from the substitution $BeCa_{0.5}Al_{-1}\square_{-0.5}$.

With rare exception, the Be contents of orthopyroxene decrease from cores of independent grains (0·7–29 ppm Be) to the rims of these grains (4–18 ppm Be) and to

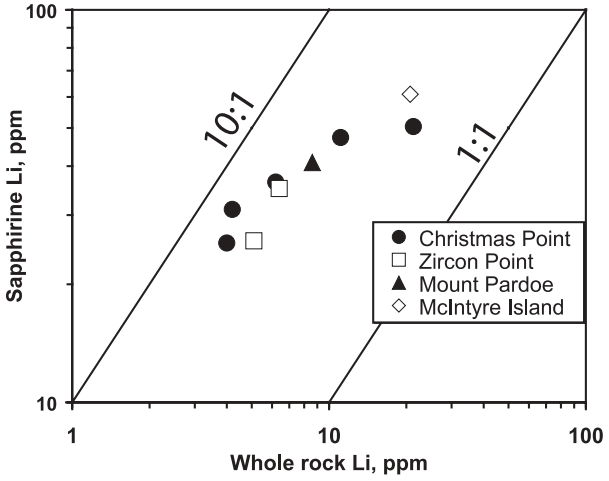

Fig. 7. Average Li content of sapphirine for a given sample as a function of whole-rock Li content of the paragneisses. Lines indicate sapphirine/bulk rock Li ratios and are for reference only.

the coronae and small grains of orthopyroxene formed by reaction of sapphirine with quartz (0·4–14 ppm Be) in any given sample (Fig. 9). Sillimanite Be content ranges from 0·1 to 26 ppm in the paragneisses. There is also a suggestion that coarse-grained sillimanite, which is texturally independent of sapphirine and might be primary, has a higher concentration of Be than secondary sillimanite in the coronae formed by reaction of sapphirine with quartz, but the textural distinction is not sufficiently clearcut to plot these separately. The maximum Be measured in this study is 37 ppm in a centimeter-sized sillimanite prism from a Christmas Point vein (sample 12263, Table 2). Be contents in plagioclase are 14–43 ppm in labradorite (An53–66), but only 0·6–15 ppm in oligoclase–andesine (An18–33). The lowest Be contents are 0·06–8 ppm in biotite, 0·2–0·6 ppm in K-feldspar (to 3 ppm in a vein), and 0·05–0·7 ppm in quartz and garnet. Preliminary analyses of spinel yield 29–43 ppm Be in 2234B and 14–25 ppm Be in 2234A.

As with the major elements, the Be concentration of each mineral (or textural variety) varies from grain to grain in a given sample, e.g. sapphirine (Fig. 8); $\pm 1\sigma$ ranges from 2% to 93%, but mostly 10–30% relative, i.e. the variation commonly exceeds the $\pm 10\%$ precision estimated for the secondary ion mass spectrometry (SIMS) measurements (see Electronic Appendices 1 and 8, available for downloading at http://www.petrology.oxfordjournals.org).

Despite grain-to-grain heterogeneity the increase of average Be content in orthopyroxene, sillimanite and biotite with increasing sapphirine Be content is systematic, particularly for coronae and small grains of secondary orthopyroxene formed by reaction of sapphirine with quartz (Fig. 10). This suggests an approach to an equilibrium distribution of Be, for which our results give the following sequence of decreasing Be content: Spr $\approx$ Crd $\gg$ Pl (An$\sim$60) $\approx$ Spl $>$ Opx I $>$ Opx II $\approx$ Sil $\approx$ Pl (An$\sim$20–30) $>$ Bt $>$ Kfs $>$ Grt $\approx$ Qtz, where I refers to relatively coarse-grained orthopyroxene and II refers to coronal and secondary orthopyroxene. Beryllium is concentrated in sapphirine by over two orders of magnitude relative to orthopyroxene and sillimanite. Our limited data suggest that Be is increasingly partitioned in plagioclase with increasing An content up to An60, whereas previous work suggested that An20–30 are the most favorable plagioclase compositions for incorporation of Be (Kosals *et al.*, 1973; Steele *et al.*, 1980; London & Evensen, 2002). Beryllium is preferentially partitioned by about an order of magnitude into sodic plagioclase relative to K-feldspar in paragneiss sample 2292L and vein sample 10514 (Table 2 and Electronic Appendix 4, available for downloading at http://www.petrology.oxfordjournals.org).

The sequence is broadly consistent with that reported for the minerals in granite (e.g. Kosals *et al.*, 1973; London & Evensen, 2002) and in high-grade metamorphic rocks from Peña Negra, Spain and Ivrea–Verbano, Italy (Bea *et al.*, 1994; Bea & Montero, 1999; Grew 2002*b*). A notable difference is that garnet in quartz-rich paragneisses of the Napier Complex contains systematically less Be than coexisting sillimanite and plagioclase.

Sapphirine Be content does not increase regularly with whole-rock Be content (Fig. 9a); this absence of a straightforward relationship is best illustrated by comparing samples 2282G and 2292M from Christmas Point, which contain virtually identical amounts of Be (Table 5). Average sapphirine Be content differs by an order of magnitude, 210 ppm and 2100 ppm, respectively, in these samples. Sapphirine constitutes several modal per cent in sample 2282G and forms grains typically 2–7 mm long, whereas in sample 2292M $<$1 modal % of fine-grained sapphirine (mostly 0·1–0·5 mm long, rarely as large as 1 mm) appears to have largely reacted away, whether in contact with quartz (Fig. 4a) or armored in sillimanite. Be enrichment in relict sapphirine is thus a phenomenon analogous to the Zn enrichment in relict staurolite (e.g. Guidotti, 1970).

WHOLE-ROCK COMPOSITION

Samples and methods

This study is based on 13 analyses of 12 quartz-rich paragneisses from Christmas Point and Mount Pardoe reported by Grew *et al.* (2000) and on new analyses using the methods described in Electronic Appendix 1 (Analytical Methods, available at http://www.petrology.oxfordjournals.org) of 14 quartz-rich paragneisses from all four localities (Table 5) and a vein from Mount Pardoe (Table 6). In addition to the 27 analyses reported in this study, we obtained Be data on 26 metamorphic

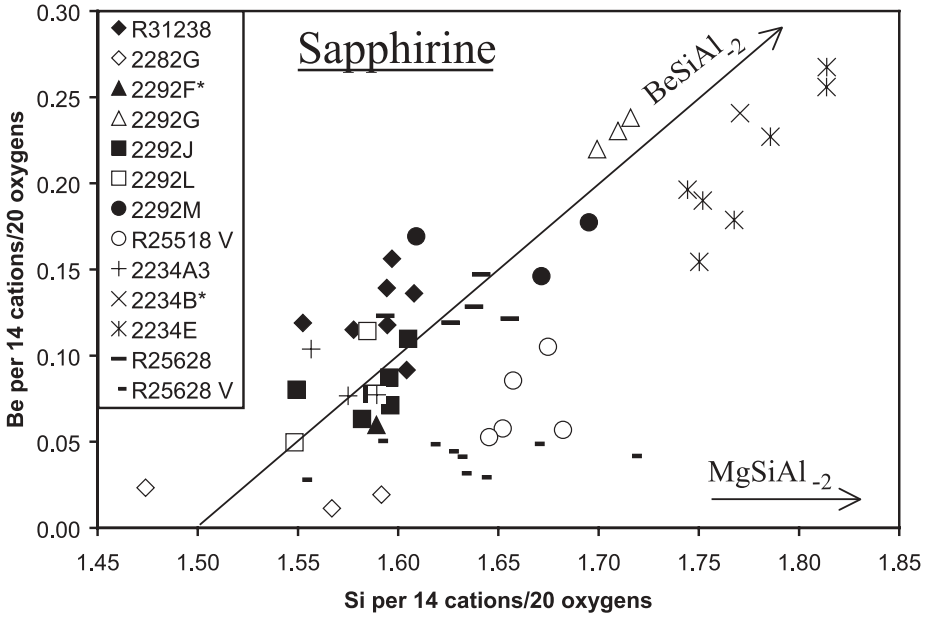

Fig. 8. Be and Si contents of individual sapphirine grains based on ion and electron microprobe data (e.g. Table 3). Asterisk indicates an average of several grains in a sample. Sapphirine with 0·025 or less Be per formula unit (except 2282G) has not been plotted. The substitution $BeSiAl_{-2}$ (inclined arrow) relates the 7:9:3 composition, $(Mg,Fe^{2+})_{3.5}(Al,Fe^{3+},Cr,V)_9Si_{1.5}O_{20}$, with an idealized khmaralite composition, $(Mg,Fe^{2+})_{3.5}(Al,Fe^{3+},Cr,V)_7BeSi_{2.5}O_{20}$. $MgSiAl_{-2}$ (horizontal arrow) is the Tschermaks substitution. V indicates anatectic veins, here interboudin pockets (R25628) and segregation related to anatectic pods (R25518); all other samples are paragneisses.

rocks from other localities in the Napier Complex, mostly the Tula Mountains (Fig. 1) and Napier Mountains to the east (Sheraton, 1980; Sheraton *et al.*, 1987); 20 analyses with $SiO_2 \geq 49{\cdot}9$ wt % are cited here (Table 7). The Christmas Point and Zircon Point veins are too coarse-grained and heterogeneous to obtain representative samples for whole-rock analysis, whereas the McIntyre Island interboudin pockets were too small and mixed with host paragneiss to extract the necessary amount (at least 15 g of homogeneous material).

Paragneisses

Although the host quartz-rich paragneisses have compositional features characteristic of pelites and psammopelites such as relatively high values of the aluminium saturation index [atomic Al/(2Ca + K + Na)] and K/(K + Na) ratio, they differ in being more magnesian: average Mg/(Mg + Fe) = 0·58 ± 0·07 (Zircon Point), 0·73 ± 0·09 (Christmas Point) and 0·75 ± 0·04 (Mount Pardoe). The paragneisses are better compared with Mg–Al-rich rocks, a controversial group typified by cordierite–orthoamphibole assemblages in the amphibolite facies. Of the several precursors proposed for Mg–Al-rich rocks, we think that volcaniclastic sediments that were hydrothermally altered by heated seawater prior to metamorphism best explain the observed geochemical features in the Napier Complex Mg–Al-rich paragneisses, a conclusion similar to that reached by Sheraton (1980). These paragneisses have several features in common with amphibolite-facies quartz–cordierite gneisses in the Archean Malene supracrustal suite, West Greenland (Dymek & Smith, 1990): high SiO_2 compared with many Mg–Al-rich rocks; Zr/TiO_2 and Y/Nb ratios that plot in the fields for rhyolite or rhyodacite–dacite; relatively low Cr, Ni and Cu contents. Cr and Ni contents are very low in all but four Napier Complex paragneiss samples; the Cr contents (from <2 ppm to 16 ppm) are characteristic of Sheraton's (1980) 'Cr-poor' group, whereas the Cr contents of the four exceptions lie in the range for his Cr-rich group (87 ppm to >1000 ppm Cr).

The Malene quartz–cordierite gneisses have pronounced negative Eu anomalies, which are characteristic of most of the analyzed Napier Complex paragneisses (Fig. 11), but not of most Archean metasedimentary rocks. The chondrite-normalized rare earth element (REE) patterns for the Napier Complex paragneisses are far more diverse than those of the Malene rocks, e.g. La_N/Yb_N values of individual samples range from 1·1 to 25·8. A feature absent in the Malene gneisses is a systematic variation of La with Th. In the samples from Christmas Point, the increase of La with Th is remarkably linear; a least-squares fit ($r^2 = 0{\cdot}997$) gives La/Th = 1·69. Because phosphorus also increases linearly with La and Th, huttonite [$CaTh(PO_4)_2$]–monazite solid solutions are probably the main carrier of Th and light REE (LREE) in these particular paragneisses.

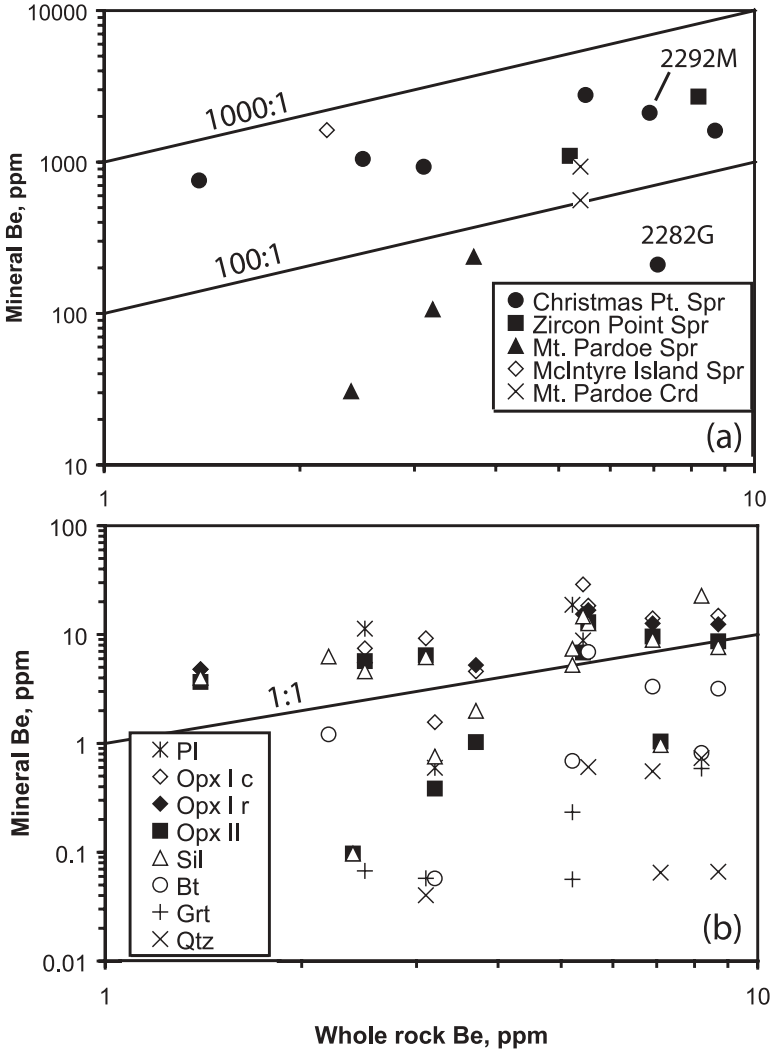

Fig. 9. Average Be content of each mineral (except individual analyses of cordierite) for a given sample as a function of whole-rock Be content of the paragneisses. Lines indicate mineral/bulk rock Be ratios and are for reference only. (a) Sapphirine and cordierite. (b) Other minerals. Ic and Ir refer to core and rim of primary orthopyroxene; II, to secondary orthopyroxene, i.e. coronae and small grains formed by reaction of sapphirine with quartz.

Compared with the Malene gneisses, the Napier Complex gneisses have higher U contents (except Mount Pardoe) and much higher Th contents (except sample 2218A), resulting in a much higher Th/U ratio for the Napier paragneisses (except sample 2218A).

Beryllium contents in 47 Napier Complex paragneisses range from below the detection limit to 9 ppm and show no systematic variation with either Al as in marine sediments (Grew, 2002*b*), Nd (28 samples), or Zr (47 samples), two relationships observed in basalts (Ryan, 2002). Compared with marine sediments (0·3–3 ppm, Grew, 2002*b*) and the great majority of pelitic and psammo-pelitic sediments and their metamorphosed equivalents, the average Be content of Napier Complex paragneisses is not unusual, 3·3 ± 2·3 ppm Be (Table 7).

Previous studies have cited evidence for a metamorphic effect on the bulk composition of the Napier Complex rocks, not only the loss of large lithophile elements (e.g. Sheraton, 1980; Sheraton & Black, 1983), but also redistribution of Sm and Nd (DePaolo *et al.*, 1982; Black & McCulloch, 1987). The very low Cs contents (≤0·3 ppm) and the variations in K/Rb ratio with K content in the paragneisses (Fig. 12) suggest that alkali loss during metamorphism was proportionally highest for Cs, intermediate for Rb and least for K. High Th/U ratios could mean that U was also lost, but the U contents are also relatively high and the high Th/U ratios could be an intrinsic feature of the precursors. Contents of P, Cu, and As are also low, but not unusually so compared with their contents in cordierite ± orthoamphibole rocks (Dymek & Smith, 1990; Smith *et al.*, 1992), which

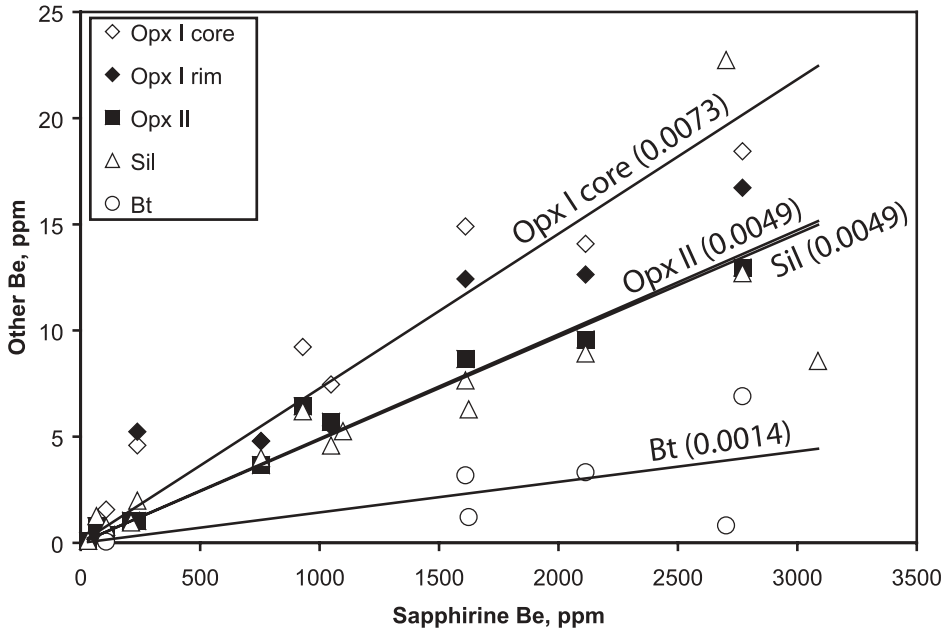

Fig. 10. Average Be content of each mineral for a given sample as a function of sapphirine Be content for a given paragneiss sample. I refers to primary orthopyroxene; II refers to secondary orthopyroxene, i.e. coronae and small grains formed by reaction of sapphirine with quartz. Lines are least-squares fits forced through the origin; the slopes are given in parentheses. The r^2 values for the fits are 0·88 for Opx I core, 0·97 for Opx II, 0·70 for Sil, and 0·35 for Bt.

are possible lower-grade equivalents. Boron is a constituent readily lost during granulite-facies metamorphism (Leeman & Sisson, 2002). Boron contents do not exceed 20 ppm, the detection limit, in any sample, and except in samples 2234A and 2234B, they probably do not exceed 4 ppm, an upper limit implied by the maximum B content of sillimanite and sapphirine, the two minerals most likely to contain B (Grew, 2002*a*). The B content of the precursor could have been one or two orders magnitude higher; e.g. the B content of Archean shales ranges from 4 to 400 ppm (Leeman & Sisson, 2002). It is less clear whether the relatively low Li contents can also be attributed to metamorphism; such a case has been made in high-grade rocks (e.g. Shaw *et al.*, 1988). The difference in average Be concentration between paragneisses containing sapphirine or primary cordierite and paragneisses lacking these minerals (Table 7) implies that the latter paragneisses could have lost Be during metamorphism.

Relationship of the veins to the host paragneisses

The questions here are whether the veins are derived from the paragneisses hosting them, and, if not, to what extent the host-rocks might have interacted with the veins during or after emplacement. Only one vein sample was suitable for analysis, sample 10514 from Mount Pardoe (Table 6). This vein has the composition of a peraluminous granite with a relatively high *mg* value, Mg/(Mg + Fe) = 0·59; its total MgO + FeO + TiO_2 of 3·44 wt % is in the upper range of the 2–4 wt % found in granites synthesized from melting of metapelites and metagraywackes (e.g. Patiño Douce & Johnston, 1991; Montel & Vielzeuf, 1997; Stevens *et al.*, 1997). The REE pattern is characterized by a marked negative Eu anomaly and high REE contents except for heavy REE (HREE; Fig. 11c). It is enriched in many other trace elements relative to the host paragneisses, notably Be, P, Cl, As, Rb, Y, Nb, Mo, Sn, Cs, Pb, Th and U; only Sc is markedly depleted (Table 6). Some of these differences can be explained in terms of the anatectic process. Order-of-magnitude enrichments of Rb, Sn and Cs, and lower K/Rb (Fig. 12) and K/Cs ratios could be due to the breakdown of biotite during anatexis and loss of these constituents to the melt, a process cited by Hall *et al.* (1993) to explain Cs concentrations in the Sardinia granite batholith. Li correlates with Sn and Cs in the Sardinia granite, but enrichment of Li in the Mount Pardoe vein is modest. Because apatite is readily soluble in peraluminous melts (e.g. Pichavant *et al.*, 1992; Wolf & London, 1994), anatexis of aluminous paragneisses should remove apatite from them, and indeed this mineral is rare in the studied paragneiss samples. Enrichment of P in the vein is consistent with dissolution of apatite in the paragneisses. The marked enrichment of the vein in Th and U could have resulted from entrainment of major rock-forming minerals that enclosed Th- and U-bearing accessories (Bea, 1996). Less obvious is the reason behind enrichment of As in

Table 5: Bulk-rock analyses of quartz-rich paragneisses

Locality:	C. Pt.	C. Pt.	C. Pt.	Z. Pt.	Z. Pt.	Z. Pt.	Z. Pt.	Z. Pt.	Z. Pt.	Mt. P.	Mt. P.	Mt. P.	Mc. I.	Mc. I.
Sample:	R25517	R31238	R31243	2234A	2234D	2234E	2234H	2234J	R31050	CC6	10503	10507	R25628	2218A
Be sink:	Spr	Spr	—	Spr	—	Spr	—	—	—	Spr	Spr	—	Spr	—
wt %														
SiO_2	78·16	78·92	76·05	77·57	75·71	79·39	76·33	77·00	80·51	63·94	73·44	79·92	73·80	54·55
TiO_2	0·61	0·53	0·85	0·17	0·53	0·17	0·58	0·20	0·15	0·26	0·31	0·24	0·35	1·21
Al_2O_3	10·20	11·30	11·16	11·83	12·07	10·95	13·34	10·82	10·85	19·44	14·38	9·06	14·70	29·62
Fe_2O_3	2·98	0·22	0·45	0·10	0·17	0	0·40	0·04	0·06	0·44	3·33	0·37	0·15	0·51
FeO	—	1·9	5·9	3·2	6·1	3·47	3·5	3·3	3·2	5·0	—	2·4	3·0	5·3
MnO	0·014	0·008	0·025	0·037	0·055	0·028	0·048	0·018	0·038	0·068	0·043	0·023	0·025	0·046
MgO	5·43	5·72	4·09	3·42	4·55	3·47	2·54	1·76	3·06	9·92	6·00	3·04	3·92	4·87
CaO	0·09	0·02	0·18	0·30	0·45	0·06	0·19	0·20	0·11	0·11	0·22	0·81	0·29	0·59
Na_2O	0·12	0·06	0·06	0·29	0·02	0·15	0·08	0·71	0·14	0·45	0·85	1·86	0·71	0·86
K_2O	1·04	0·73	0·93	3·09	0·17	1·79	1·23	5·79	1·61	0·79	1·21	1·88	2·23	1·69
P_2O_5	0·038	0·037	0·051	0·004	0·042	0·003	0·009	0·012	0·007	0·011	0·008	0·031	0·024	0·030
SO_3	0·032	0·047	0·043	0·044	0·056	0·041	0·053	0·043	0·042	0·045	<0·015	0·046	0·044	0·044
CO_2	—	0·25	0·25	0·14	0·03	0·12	0·18	0·39	0·17	0·36	—	0·09	0·23	0·10
H_2O^-	—	0·09	0·09	0·09	0·09	0·08	0·10	0·06	0·09	0·10	—	0·17	0·18	0·20
H_2O^+	—	0·31	0·52	0·54	0·69	0·56	0·55	0·07	0·41	0·28	—	0·51	0·65	0·70
F	0·09	0·19	0·13	0·34	0·13	0·43	0·08	0·04	0·29	0·03	0·05	0·01	0·51	0·10
O = F,Cl	−0·04	−0·08	−0·06	−0·15	−0·05	−0·18	−0·04	−0·02	−0·13	−0·01	−0·02	−0·01	−0·22	−0·04
Total	98·96	100·48	100·96	101·13	100·93	100·63	99·27	100·62	100·72	101·34	99·93	100·57	100·72	100·50
ppm (except Eu, which is in ppb)														
Li	—	4·2	7·1	6·4	5·6	5·1	3·6	4·0	5·4	8·6	—	9·0	20·7	17·9
Be	6·41	8·7	1·9	5·2	2·8	8·2	1·4	2·7	8·2	3·2	2·40	2·9	2·2	2·3
B	—	<20	<20	<20	<20	<20	<20	<20	<20	<20	—	<20	<20	<20
F	863	1915	1265	3415	1253	4270	821	400	2948	278	492	121	5079	976
Cl	384	118	184	72	<5	106	29	105	128	6	179	<5	205	116
Sc	13·33	11	14	4	12	5	11	6	5	9	6·20	4	13	32
V	14	9	30	<3	86	<3	135	<3	<3	23	26	21	93	410
Cr	<13	<2	<2	<2	89	<2	542	<2	<2	<2	<10	2	189	898
Ni	13·97	13	16	34	43	19	36	16	20	25	13·60	19	106	92
Cu	2·47	4	6	6	31	4	33	6	4	9	162·93	8	4	12
Zn	12·75	18·1	20·7	66·6	99·0	44·2	72·8	24·3	69·8	101·6	48·45	49·8	31·7	41·9
Ga	16·16	18·5	16·3	23·8	21·8	22·0	17·7	15·4	21·5	36·6	21·64	11·5	19·5	48·6
Ge	<1·5	0·8	0·9	1·3	1·3	1·4	1·6	1·0	1·3	1·0	<1·5	0·8	1·1	2·4
As	1·01	1·0	0·9	1·2	0·6	1·3	1·3	0·9	0·9	0·6	<1·5	1·1	1·0	0·6
Br	—	<1	<1	<1	<1	<1	<1	<1	<1	1	—	<1	<1	<1
Rb	17·15	12·2	16·2	85·8	5·1	69·4	30·1	104·6	65·6	8·8	12·39	63·2	43·7	34·9
Sr	4·77	16·1	17·4	30·8	15·4	17·0	34·2	35·9	19·2	21·3	13·79	38·9	30·4	32·2
Y	46·34	101·0	165·7	162·9	221·2	171·9	10·0	60·1	196·4	29·4	48·53	20·2	121·1	242·8
Zr	579·31	676	602	319	365	287	213	310	292	308	206·63	287	188	301
Nb	27·59	30·4	40·6	69·3	55·0	70·0	18·2	20·9	50·3	1·7	2·99	15·3	31·1	160·3
Mo	0·50	0	0	1·5	5·1	1·5	2·6	0	1·5	0	0·67	1·4	0·4	11·3
Ag	0·53	<0·01	<0·01	<0·01	<0·01	<0·01	<0·01	<0·01	<0·01	<0·01	<0·2	<0·01	<0·01	0·02
Cd	0·82	<0·05	<0·05	<0·05	0·13	<0·05	0·05	<0·05	<0·05	<0·05	0·54	0·12	<0·05	0·15
Sn	3·23	4·0	4·1	1·7	4·1	1·2	1·1	1·9	2·1	1·9	1·64	4·5	2·9	6·8
Sb	<0·2	0	0	0	0	0	0	0	0	0	<0·2	0	0	0·1
Cs	<0·1	0·11	0·09	0·14	0·09	0·16	0·13	0·12	0·14	0·09	<0·1	0·18	0·14	0·15

Table 5: Continued

Locality:	C. Pt.	C. Pt.	C. Pt.	Z. Pt.	Z. Pt.	Z. Pt.	Z. Pt.	Z. Pt.	Z. Pt.	Mt. P.	Mt. P.	Mt. P.	Mc. I.	Mc. I.
Sample:	R25517	R31238	R31243	2234A	2234D	2234E	2234H	2234J	R31050	CC6	10503	10507	R25628	2218A
Be sink:	Spr	Spr	—	Spr	—	Spr	—	—	—	Spr	Spr	—	Spr	—
Ba	342·95	379	792	191	19	90	381	813	89	188	327·82	376	346	276
La	81·54	118·90	104·60	46·48	102·60	31·27	18·86	45·89	45·44	39·77	48·08	78·72	55·69	34·93
Ce	165·23	247·20	206·00	82·02	194·00	69·63	32·58	62·03	85·11	84·19	77·58	151·40	113·00	65·51
Pr	18·86	26·84	21·92	7·61	19·98	6·93	3·07	4·99	9·61	9·08	7·24	15·02	11·84	5·10
Nd	72·60	101·4	83·37	27·88	71·83	26·97	11·14	16·75	37·97	34·53	24·47	51·56	45·02	18·35
Sm	12·11	21·76	18·23	9·92	16·83	9·04	2·71	5·01	12·12	6·70	4·11	7·77	11·38	9·69
Eu	1305	2144	3217	961	872	518	930	1540	614	608	1392	1106	803	1174
Gd	11·34	24·30	21·11	17·49	25·45	17·03	2·98	10·09	20·40	8·76	3·69	5·82	17·49	30·52
Tb	1·33	3·98	3·97	3·95	5·34	4·23	0·44	2·01	4·57	1·50	0·75	0·77	3·38	7·77
Dy	9·78	19·41	24·57	24·90	32·57	27·93	2·00	11·29	29·21	8·82	6·97	3·81	21·23	52·79
Ho	1·58	3·85	5·66	6·04	7·14	6·54	0·37	2·34	6·83	1·96	1·56	0·70	4·26	10·63
Er	5·41	10·19	17·33	19·38	21·78	20·04	0·98	6·52	21·23	5·96	6·56	2·08	13·44	30·73
Tm	0·88	—	—	—	—	—	—	—	—	—	1·09	—	—	—
Yb	5·43	8·99	16·23	19·71	20·19	19·17	0·92	5·50	19·85	5·82	7·78	2·07	11·98	22·40
Lu	0·95	1·35	2·44	3·11	2·92	2·73	0·15	0·84	2·98	0·87	1·29	0·29	1·65	2·73
Hf	15·06	17·7	15·4	13·6	13·1	11·7	5·6	11·1	12·6	13·1	7·55	9·5	7·2	9·7
Ta	2·25	4·3	4·9	6·2	6·5	6·3	4·4	2·6	5·9	1·9	0·35	1·1	4·3	14·8
Pb	8·46	13·1	13·7	24·6	10·4	20·6	6·7	17·0	20·3	18·9	9·42	20·4	11·4	3·4
Bi	0·18	0	0	0	0	0	0·1	0	0	0	<0·1	0	0	0
Th	42·58	65·8	55·4	94·9	51·0	91·9	6·7	49·3	86·8	47·5	22·31	22·7	42·3	2·2
U	3·89	7·30	4·10	15·66	10·40	15·65	0·92	3·13	11·08	1·92	0·99	1·39	3·04	8·14
mg no.	0·78	0·83	0·54	0·65	0·56	0·64	0·54	0·48	0·63	0·77	0·78	0·66	0·69	0·60
ASI	6·87	12·11	7·83	2·71	11·68	4·80	7·35	1·38	5·02	10·78	4·62	1·38	3·59	6·87
La_N/Yb_N	10·21	8·98	4·38	1·60	3·45	1·11	13·93	5·67	1·56	4·64	4·20	25·83	3·16	1·06
Eu/Eu*	0·34	0·28	0·50	0·22	0·13	0·13	1·00	0·66	0·12	0·24	1·09	0·50	0·17	0·21

Localities: C. Pt., Christmas Point; Z. Pt., Zircon Point; Mt. P., Mount Pardoe; Mc. I., McIntyre Island. Be sink, sapphirine (Spr); neither sapphirine nor primary cordierite (—); cordierite in sample 10507 is secondary. *mg* no. = Mg/(Mg + Fe); ASI (aluminum saturation index) = Al/(2Ca + K + Na).

the vein; breakdown of sulfide during anatexis is a possible explanation.

None of the explanations cited above preclude the possibility that the present host-rocks are residua after removing melts comparable with the analyzed vein at Mount Pardoe, a model proposed by Grew *et al.* (2000). Another compositional feature consistent with this model is the vein REE pattern (Fig. 11c), which implies the presence of K-feldspar, plagioclase and garnet in its residua; these minerals are present in the host paragneisses, the feldspars as components of mesoperthite. Although the vein contains more Al_2O_3 than most of the host paragneisses, it has a lower ASI index, and thus Al_2O_3 content, by itself, does not exclude the possibility that the host paragneisses are residua for this vein. However, the relatively high TiO_2 content is not consistent with a local origin for the Mount Pardoe veins. The analyzed vein contains substantially more TiO_2 than the host-rocks, whereas most experiments give melts containing less TiO_2 than the melted material (Vielzeuf & Holloway, 1988; Patiño Douce & Johnston, 1991; Vielzeuf & Montel, 1994; Montel & Vielzeuf, 1997; Stevens *et al.*, 1997). It has been suggested that the high TiO_2 content could be due to wall-rock contamination, but the host-rocks contain less TiO_2 than the vein, so contamination seems unlikely, and their entrainment could not enrich the melt in TiO_2. More probably, the high TiO_2 content is related to high temperature of melting of a metasediment richer in Ti than the hosts to the veins. In most of the experiments cited above, TiO_2 increases with temperature of melting. Thus, an explanation consistent with the experimental

Table 6: Average compositions of paragneisses compared to vein at Mount Pardoe

	Paragneiss			Vein†
	Average*	*Stdev**	*n*	10514 ($n = 1$)
wt %				
SiO_2	72·94	5·5	7	67·29
TiO_2	0·22	0·1	7	1·19
Al_2O_3	14·13	3·7	7	17·04
Fe_2O_3	0·92	0·5	6	0·16
FeO	2·76	1·1	6	1·10
MnO	0·04	0·0	7	0·011
MgO	6·28	2·2	7	1·01
CaO	0·34	0·2	7	1·10
Na_2O	1·03	0·5	7	2·74
K_2O	1·24	0·3	7	6·71
P_2O_5	0·02	0·0	7	0·543
SO_3	0·01	0·0	7	0·049
ppm (except Eu, which is in ppb)				
Li	8·0	0·8	6	12·1
Be	3·2	1·1	7	11·4
F	213·0	141·3	7	431
Cl	40·4	64·8	7	353
Sc	6·5	1·6	7	<2
V	16·3	7·0	7	13
Cr	2·0	1·6	7	<2
Ni	15·1	5·2	7	16
Cu	28·0	59·5	7	40
Zn	73·2	18·7	7	34·9
Ga	24·9	7·5	7	23·3
As	0·2	0·4	7	7·8
Br	0·4	0·4	7	<1
Rb	19·1	19·8	7	390
Sr	19·0	10·3	7	44·6
Y	40·1	17·5	7	152·7
Zr	246·8	39·5	7	461
Nb	4·3	5·1	7	64·1
Mo	0·8	0·5	7	10·1
Sn	1·6	1·4	7	24·8
Cs	0·04	0·07	7	5·04
Ba	249·7	83·9	7	319
La	56·3	24·6	7	109·1
Ce	102·7	43·1	7	349·4
Pr	8·9	5·4	7	46·61
Nd	31·7	14·8	7	196·6
Sm	6·2	1·9	3	62·33
Eu	1036	397	3	1176
Gd	6·1	2·5	3	72
Tb	1·0	0·4	3	11·45
Dy	6·5	2·5	3	45·6
Ho	1·4	0·6	3	5·44
Er	4·9	2·4	3	8·86
Yb	5·2	2·9	3	2·31
Lu	0·8	0·5	3	0·18
Hf	9·8	2·0	7	17·7
Ta	1·7	0·8	7	3·1
Pb	11·6	5·6	7	130·8
Bi	0·0	0·1	7	0·8
Th	30·5	9·3	7	338·5
U	1·5	0·4	7	77·36
mg	0·75	0·0	7	0·59
ASI	4·99	3·3	7	1·24
k	0·46	0·1	7	0·62
La_N/Yb_N	11·6	12·4	3	32·1
Eu/Eu*	0·61	0·43	3	0·054

mg = Mg/(Mg + Fe), ASI (aluminum saturation index) = Al/(2Ca + K + Na), *k* = K/(K + Na).
*From Grew *et al.* (2000) and Table 5; sample 10502a not included.
†Also H_2O^+ 0·2, H_2O^- 0·14, CO_2 0·04 wt %, B < 20, Ge 1·2, Ag < 0·1, Sb 0·1 ppm; Sum 99·28 wt %.

data is that the veins are granitic melts formed at $T > 1000°C$ of a source containing ~1 wt % TiO_2, a content not much greater than the maximum TiO_2 in the Malene quartz–cordierite gneisses and Orijärvi cordierite–orthoamphibole gneisses, 0·8 wt % (Dymek & Smith, 1990; Smith *et al.*, 1992). The FeO and MgO contents of the experimental melts also increase with temperature, albeit less consistently than TiO_2, so high temperatures, rather than wall-rock contamination or entrainment, could also be invoked to explain the relatively high FeO + MgO content of the vein. An independent indication of high temperature is the Zr content of 461 ppm, which indicates 900°C, assuming zircon saturation in the vein ($M = 1·28$, Hanchar & Watson, 2003).

In summary, we now consider the model of local origin (Grew *et al.*, 2000) for the Mount Pardoe vein to be in error; it appears that rocks other than the host paragneisses contributed the melt, and neither the major nor the trace element data exclude this possibility, i.e. most of the geochemical data are consistent with both models. The roles of fractionation, differentiation and wall-rock

Table 7: Average beryllium concentrations in Napier Complex paragneisses

Be sink	Beryllium, ppm (± 1σ)	*n*
Christmas Pt., Zircon Pt., Mt. Pardoe (25 samples, average 4·0 ± 2·4 ppm Be)		
Sapphirine ± cordierite	4·9 ± 2·4	13
None*	2·9 ± 2·1	12
All sampled localities (47 samples, $SiO_2 \geq 49{\cdot}9$ wt %, average 3·3 ± 2·3 ppm Be)		
Sapphirine ± cordierite	4·0 ± 2·4	22
Primary cordierite only	3·5 ± 2·4	6
None*	2·5 ± 1·8	19

*These samples contain cordierite replacing osumilite as given by Sheraton *et al*. (1987, appendix 1), and clearly secondary cordierite in samples 2292H, 2292J, 10507 and 10513. Sources: Table 5; Ellis *et al*. (1980); Sheraton (1980); Sheraton *et al*. (1987); Grew *et al*. (2000).

contamination also cannot be discounted. For example, fractionation could have contributed to the negative Eu anomaly and enrichment of incompatible elements such as Th as reported by Sawyer (1987). The presence of chlorapatite and wagnerite in the vein described by Grew *et al.* (2000) and Roy *et al.* (2003) probably resulted from differentiation of the melt following anatexis.

There is less doubt concerning the origin of the beryllium pods at Christmas Point and Zircon Point, where the preponderance of evidence indicates that they are not locally derived. The Zircon Point pod has discolored the host paragneiss (Grew, 1981) and the pods at both localities stand out from their metasedimentary hosts more than do the veins at Mount Pardoe (e.g. Fig. 2c). The presence of distinct quartz cores with beryllium minerals surrounded by a microcline-rich margin is good evidence for differentiation prior to emplacement at Christmas Point, as are the segregations of wagnerite and apatite-group minerals in the Christmas Point pods described by Grew *et al.* (2000) and Roy *et al.* (2003). In summary, the beryllium veins did not result from melting of the layers presently hosting them, but of several more distant rock layers; they were then emplaced into their present hosts, which provided loci favorable for accumulation of melt. These host-rocks appear to have been more competent than associated rocks and pulled apart, opening up spaces for melts to intrude, one of the processes considered essential for segregating melts from their source rocks and transporting them away (e.g. Sawyer, 1994, 2001).

BERYLLIUM AND THE MELTING PROCESS

London & Evensen (2002) and Evensen & London (2003) predicted that residua containing the Be sink cordierite would retain Be, whereas associated granitic melts would be too depleted in Be for beryl to appear in pegmatites resulting from fractionation of the melts. The capacity of sapphirine to retain Be is evidenced by the average Be contents of paragneisses containing sapphirine being 160–170% the average Be contents of paragneisses lacking both sapphirine and primary cordierite (Table 7). The relationship between Be content and presence of sapphirine is consistent with a major role for sapphirine in retaining Be during anatexis. Thus, neither sapphirine nor cordierite could have have been residual phases in the source rocks of the Be-rich veins.

There is also no evidence that Be concentrations in the veins could have originated from the host paragneisses by another process. As in the case of Ti, the rocks hosting the veins at Mount Pardoe contain less Be than the vein, so contamination by the host paragneisses or their entrainment are implausible explanations for the presence of surinamite in the veins. Concentration of Be in the quartz cores of the Christmas Point pods implies that Be was already present when the pods differentiated and was not incorporated by remobilization of Be from the host-rocks after emplacement of the pods.

Even in the absence of sapphirine and cordierite, not all Be would have been lost to melt. Most of the Napier Complex rocks analyzed for Be and lacking sapphirine and primary cordierite contain sillimanite or orthopyroxene, which incorporate moderate amounts of Be (Figs 9 and 10). Their presence could explain the retention of some Be in these paragneisses, yet formation of these minerals in the residua would not prevent a portion of the Be being released into the melt.

None the less, another mineral might have played a critical role—biotite; its breakdown would have released Be into the melt. Although biotite is sparse in the paragneisses analyzed in this study, it might have been more abundant in the source rocks of the veins. A major role for biotite is suggested by the Be budget in the paragneisses and discordant leucosomes in the Ivrea–Verbano Zone, Italy, where metapelite whole-rock Be concentration decreases from 2·34 ± 1·05 ppm in the amphibolite facies to 0·48 ± 0·27 ppm in the granulite facies (Bea & Montero, 1999). Except at the highest grade of metamorphism, whole-rock Be concentration tracks biotite mode much more closely than it does the modes of either plagioclase or sillimanite, other potential carriers of Be (Fig. 9). Biotite must have been the main carrier of Be in the Ivrea–Verbano Zone. The Napier Be veins could have originated in a source rock

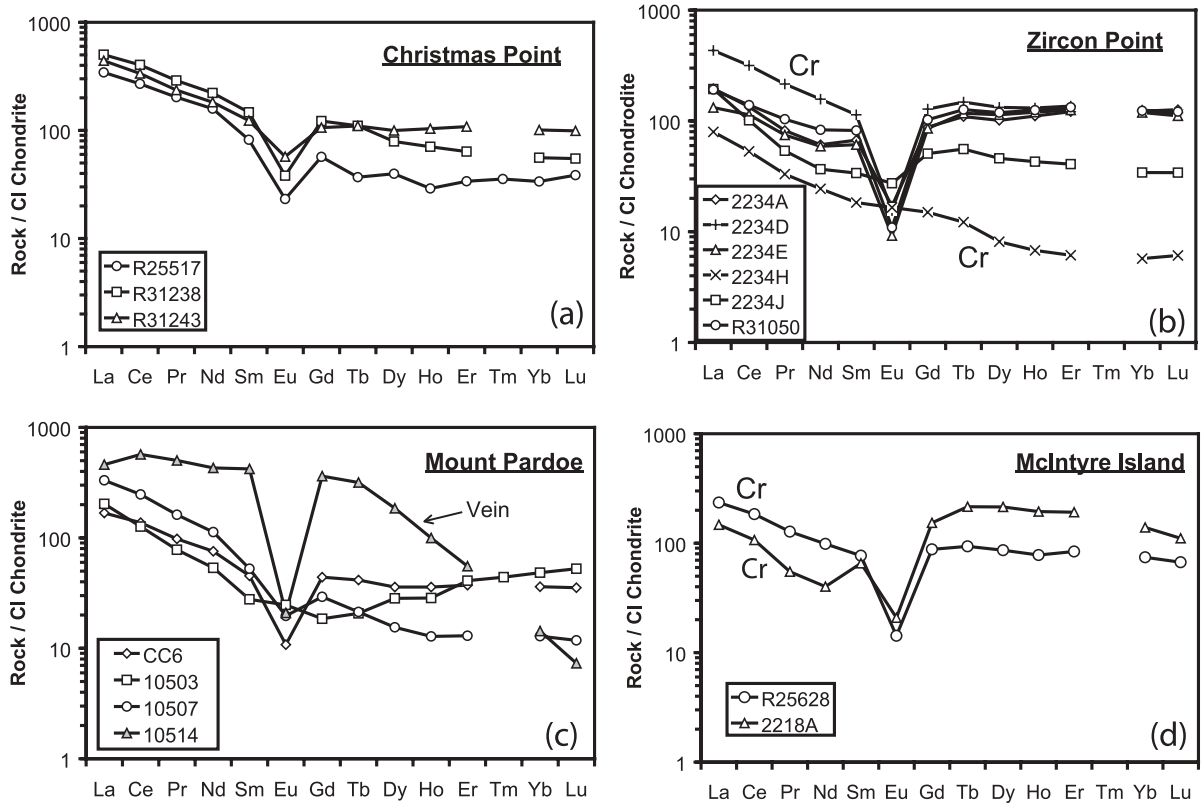

Fig. 11. REE diagrams for the rocks for which complete REE data are available from Christmas Point, Zircon Point, Mount Pardoe and McIntyre Island (Tables 5 and 6). Normalization based on McDonough & Sun (1995). Cr indicates high-Cr varieties.

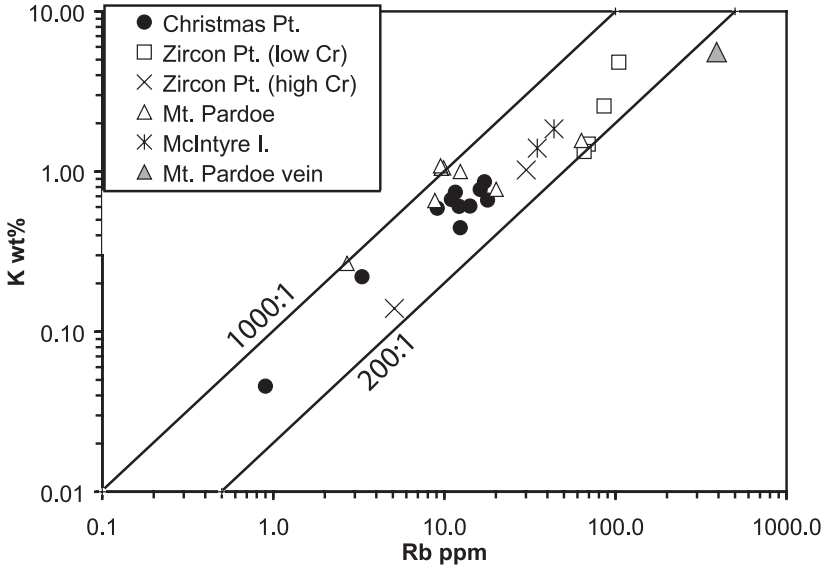

Fig. 12. Potassium vs Rb contents and ratios for the 27 paragneisses and one vein reported by Grew *et al.* (2000) and in Tables 5 and 6.

as rich in biotite as the Ivrea–Verbano metapelite, and one where biotite similarly dominated the Be budget. The higher Cs, Rb, Ti and Sn contents and lower K/Cs and K/Rb ratios in the Mount Pardoe veins compared with their host paragneisses constitute further evidence for a biotite-rich source.

We now return to the question of why there are veins with beryllium minerals in the Napier Complex and

not in other granulite-facies terrains, even in Archean complexes with similar Mg–Al-rich paragneisses or with sapphirine–quartz assemblages characteristic of UHT metamorphism. An important factor is the relatively high Be concentrations in the precursors in the Mg–Al-rich paragneisses. We suggest that the average Be concentration of sapphirine-bearing paragneisses (5 ppm Be at the three localities where Be veins are found, Table 7) could be more representative of the Be content of the protoliths from which the veins were derived than the average Be concentration of all analyzed paragneisses from these localities (4 ppm Be), because rocks lacking sapphirine and cordierite may have lost Be to the melt during anatexis. An average concentration of 5 ppm Be in the precursors is nearly twice the 3 ppm for average pelite cited by Evensen & London (2003) as the source of a granite system that yields beryl-bearing pegmatites. Equally important could be the conditions under which the source rocks were melted. London & Evensen (2002) and Evensen & London (2003) concluded that for anatexis under amphibolite-facies conditions in the absence of cordierite, the bulk distribution coefficient for Be between minerals in pelitic source rocks and granitic melt is less than unity, so that Be concentration in the melt increases to 4–6 ppm. However, the conditions for melting could have been different under UHT conditions and it is possible that the resulting melts would be more enriched in Be than under the amphibolite-facies conditions discussed by London & Evensen. The marked loss of Be in the metapelites of the Ivrea–Verbano zone (Bea & Montero, 1999; Grew, 2002*b*), in the transition from the amphibolite to the granulite facies, suggests that higher temperatures could have a more drastic effect on the distribution of Be between melt, source and restite. The third factor is fractionation of the melt to generate residual liquids sufficiently enriched in Be for beryllian sapphirine to be precipitated. Evensen & London (2003) concluded that a three-stage process with extended fractionation was necessary to achieve a granitic liquid containing at least 70 ppm Be, enough to precipate beryl from an anatectic magma containing 4–6 ppm Be. Although the Napier Complex veins have undergone some fractionation, it is unlikely that they are the result of such extreme fractionation, and for this reason we think that the source was richer in Be than typical pelite and that the anatectic process more efficient in extracting Be under UHT conditions. It is possible that the Be concentration in the melt required for beryllian sapphirine saturation is less than the 70 ppm required for beryl saturation, which would further reduce the need for so many stages and such extended fractionation to yield the veins containing Be minerals.

SUMMARY

In most granulite-facies metamorphic complexes, Be is rare trace element that does not manifest itself. However, the protoliths of the Napier Complex Mg–Al-rich paragneisses contained sufficient Be for this constituent to be manifested after UHT metamorphism and anatexis, i.e. 5 ppm Be on the average vs 3 ppm in typical pelite. Not only is Be a significant constituent in sapphirine (to 1 wt % BeO), an important rock-forming mineral in Mg–Al-rich varieties of Napier Complex paragneisses, but also Be minerals are present in veins formed by anatexis during the granulite-facies event. The present distribution of Be in Napier Complex paragneisses and anatectic veins resulted from both the mechanical properties of the rocks during deformation and from the capacity of sapphirine and cordierite to concentrate Be. Like cordierite, sapphirine is a highly favorable host for Be, and thus rocks containing either mineral should retain their Be content, even at ultrahigh temperatures and during extensive melting. However, paragneisses lacking sapphirine and cordierite, but richer in biotite, lost Be to anatectic melts. Biotitic gneisses were probably less competent than the sapphirine-bearing gneisses, so the melts were drawn to the latter and collected in spaces opened during deformation and boudinage of the more competent paragneisses. Fractionation of the melts concentrated Be to the extent that Be minerals could crystallize. The final result was anatectic veins containing high-temperature Be minerals hosted by relatively Be-rich sapphirine-bearing paragneisses.

ACKNOWLEDGEMENTS

We thank participants of the Australian National Antarctic Research Expedition and the 40th Japanese Antarctic Research Expedition for logistics support in the fieldwork and collecting in 1979–1980 and 1999, respectively. Particular thanks go to K. Shiraishi (National Institute of Polar Research) and to the captain and crew of the icebreaker *Shirase* for arranging a helicopter flight to Christmas Point in January 1999. We also thank Chris Carson for sample CC6 from Mount Pardoe; Dan Dunkley for observations on the structures, fruitful discussions in the field, and photographs of pods at Christmas Point; Chris Wilson for samples R31050, R31238 and R31243 and supporting documentation; Andrew Christy and Ulrich Senff for arranging the geochemical analyses at Geoscience Australia and the Australian National University; Tony Phimphisane for assistance with sample preparation; Joseph Evensen for Be-doped glasses; Darrell Henry for the Excel worksheet for calculating isotherms from biotite compositions; Simon Harley for permission to cite unpublished data from his field notes; Anthony Higgins for loan of sample

339313, magnesiotaaffeite-6*N*′3*S* (musgravite) from Dove Bugt, East Greenland; Julie Hollis for permission to cite unpublished material in her Ph.D. thesis. The thoughtful and insightful reviews of Julia Baldwin, Ron Frost, Simon Harley, Julie Hollis, John Schumacher and an anonymous referee are much appreciated. E.S.G.'s and M.G.Y.'s research was supported by US National Science Foundation grants OPP-9813569, OPP-00887235 and MRI-0116235 to the University of Maine.

REFERENCES

Barbier, J., Grew, E. S., Moore, P. B. & Su, S.-C. (1999). Khmaralite, a new beryllium-bearing mineral related to sapphirine: a superstructure resulting from partial ordering of Be, Al and Si on tetrahedral sites. *American Mineralogist* **84**, 1650–1660.

Bea, F. (1996). Residence of REE, Y, Th and U in granites and crustal protoliths; implications for the chemistry of crustal melts. *Journal of Petrology* **37**, 521–552.

Bea, F. & Montero, P. (1999). Behavior of accessory phases and redistribution of Zr, REE, Y, Th, and U during metamorphism and partial melting of metapelites in the lower crust: an example from the Kinzigite Formation of Ivrea–Verbano, NW Italy. *Geochimica et Cosmochimica Acta* **63**, 1133–1153.

Bea, F., Pereira, M. D. & Stroh, A. (1994). Mineral/leucosome trace-element partitioning in a peraluminous migmatite (a laser ablation–ICP–MS study). *Chemical Geology* **117**, 291–312.

Black, L. P. & McCulloch, M. T. (1987). Evidence for isotopic equilibration of Sm–Nd whole-rock systems in early Archaean crust of Enderby Land, Antarctica. *Earth and Planetary Science Letters* **82**, 15–24.

Black, L. P., James, P. R. & Harley, S. L. (1983). Geochronology and geological evolution of metamorphic rocks in the Field Islands area, East Antarctica. *Journal of Metamorphic Geology* **1**, 277–303.

Carson, C. J., Ague, J. J., Grove, M., Coath, C. D. & Harrison, T. M. (2002). U–Pb isotopic behaviour of zircon during upper-amphibolite facies fluid infiltration in the Napier Complex, east Antarctica. *Earth and Planetary Science Letters* **199**, 287–310.

Christy, A. G., Tabira, Y., Hölscher, A., Grew, E. S. & Schreyer, W. (2002). Synthesis of beryllian sapphirine in the system MgO–BeO–Al_2O_3–SiO_2–H_2O and comparison with naturally occurring beryllian sapphirine and khmaralite. Part 1: Experiments, TEM and XRD. *American Mineralogist* **87**, 1104–1112.

DePaolo, D. J., Manton, W. I., Grew, E. S. & Halpern, M. (1982). Sm–Nd, Rb–Sr, and U–Th–Pb systematics of granulite facies rocks from Fyfe Hills, Enderby Land, Antarctica. *Nature* **298**, 614–618.

Dymek, R. F. & Smith, M. S. (1990). Geochemistry and origin of Archaean quartz–cordierite gneisses from the Godthåbsfjord region, West Greenland. *Contributions to Mineralogy and Petrology* **105**, 715–730.

Ellis, D. J., Sheraton, J. W., England, R. N. & Dallwitz, W. B. (1980). Osumilite–sapphirine–quartz granulites from Enderby Land, Antarctica—mineral assemblages and reactions. *Contributions to Mineralogy and Petrology* **72**, 123–143.

Evensen, J. M. & London, D. (2002). Experimental silicate mineral/melt partition coefficients for beryllium and the crustal Be cycle from migmatite to pegmatite. *Geochimica et Cosmochimica Acta* **66**, 2239–2265.

Evensen, J. M. & London, D. (2003). Experimental partitioning of Be, Cs, and other trace elements between cordierite and felsic melt, and the chemical signature of S-type granite. *Contributions to Mineralogy and Petrology* **144**, 739–757.

Grew, E. S. (1980). Sapphirine + quartz association from Archean rocks in Enderby Land, Antarctica. *American Mineralogist* **65**, 821–836.

Grew, E. S. (1981). Surinamite, taaffeite and beryllian sapphirine from pegmatites in granulite-facies rocks of Casey Bay, Enderby Land, Antarctica. *American Mineralogist* **66**, 1022–1033.

Grew, E. S. (1982). Osumilite in the sapphirine–quartz terrane of Enderby Land, Antarctica: implications for osumilite petrogenesis in the granulite facies. *American Mineralogist* **67**, 762–787.

Grew, E. S. (1998). Boron and beryllium minerals in granulite-facies pegmatites and implications of beryllium pegmatites for the origin and evolution of the Archean Napier Complex of East Antarctica. *Memoirs of the National Institute of Polar Research Special Issue* **53**, 74–92.

Grew, E. S. (2002*a*). Borosilicates (exclusive of tourmaline) and boron in rock-forming minerals in metamorphic environments. In: Grew, E. S. & Anovitz, L. M. (eds) *Boron: Mineralogy, Petrology, and Geochemistry*. *Mineralogical Society of America, Reviews in Mineralogy* **33**, 387–502 (second printing with corrections and additions).

Grew, E. S. (2002*b*). Beryllium in metamorphic environments (emphasis on aluminous compositions). In: Grew, E. S. (ed.) *Beryllium: Mineralogy, Petrology, and Geochemistry*. *Mineralogical Society of America, Reviews in Mineralogy and Geochemistry* **50**, 487–549.

Grew, E. S., Chernosky, J. V., Werding, G., Abraham, K., Marquez, N. & Hinthorne, J. R. (1990). Chemistry of kornerupine and associated minerals, a wet chemical, ion microprobe, and X-ray study emphasizing Li, Be, B and F contents. *Journal of Petrology* **31**, 1025–1070.

Grew, E. S., Yates, M. G., Barbier, J., Shearer, C. K., Sheraton, J. W., Shiraishi, K. & Motoyoshi, Y. (2000). Granulite-facies beryllium pegmatites in the Napier Complex in Khmara and Amundsen Bays, western Enderby Land, East Antarctica. *Polar Geoscience* **13**, 1–40.

Guidotti, C. V. (1970). The mineralogy and petrology of the transition from the lower to upper sillimanite zone in the Oquossoc area, Maine. *Journal of Petrology* **11**, 277–336.

Hall, A., Jarvis, K. E. & Walsh, J. N. (1993). The variation of cesium and 37 other elements in the Sardinian granite batholith, and the significance of cesium for granite petrogenesis. *Contributions to Mineralogy and Petrology*, **114**, 160–170.

Hanchar, J. M. & Watson, E. B. (2003). Zircon saturation thermometry. In: Hanchar, J. M. & Hoskin, P. W. O. (eds) *Zircon. Reviews in Mineralogy and Geochemistry* **53**, 89–112.

Harley, S. L. (1985). Paragenetic and mineral–chemical relationships in orthoamphibole-bearing gneisses from Enderby Land, east Antarctica: a record of Proterozoic uplift. *Journal of Metamorphic Geology* **3**, 179–200.

Harley, S. L. (2004). Extending our understanding of ultrahigh temperature crustal metamorphism. *Journal of Mineralogical and Petrological Sciences* **99**, 140–158.

Harley, S. L. & Motoyoshi, Y. (2000). Al zoning in orthopyroxene in a sapphirine quartzite: evidence for >1120°C UHT metamorphism in the Napier Complex, Antarctica, and implications for the entropy of sapphirine. *Contributions to Mineralogy and Petrology* **138**, 293–307.

Henry, D. J., Guidotti, C. V. & Thomson, J. A. (2005). The Ti-saturation surface for low-to-medium pressure metapelitic biotites: implications for geothermometry and Ti-substitution mechanisms. *American Mineralogist* **90**, 316–328.

Hollis, J. A. (2000). Natural and experimental constraints on ultra-high temperature metamorphism. Ph.D. thesis, University of Edinburgh.

Hölscher, A., Schreyer, W. & Lattard, D. (1986). High-pressure, high-temperature stability of surinamite in the system MgO–BeO–Al_2O_3–SiO_2–H_2O. *Contributions to Mineralogy and Petrology* **92**, 113–127.

Kosals, Ya. A., Nedashkovskiy, P. G., Petrov, L. L. & Serykh, V. I. (1973). Beryllium distribution in granitoid plagioclase. *Geochemistry International* **10**, 753–767.

Leeman, W. P. & Sisson, V. B. (2002). Geochemistry of boron and its implications for crustal and mantle processes. In: Grew, E. S. & Anovitz, L. M. (eds) *Boron: Mineralogy, Petrology, and Geochemistry*. *Mineralogical Society of America, Reviews in Mineralogy* **33**, 645–708 (second printing with corrections and additions).

London, D. & Evensen, J. M. (2002). Beryllium in silicic magmas and the origin of beryl-bearing pegmatites. In: Grew, E. S. (ed.) *Beryllium: Mineralogy, Petrology, and Geochemistry*. *Reviews in Mineralogy and Geochemistry* **50**, 445–486.

McDonough, W. F. & Sun, S.-S. (1995). The composition of the Earth. *Chemical Geology* **120**, 223–253.

Montel, J.-M. & Vielzeuf, D. (1997). Partial melting of metagreywackes, Part II. Compositions of minerals and melts. *Contributions to Mineralogy and Petrology* **128**, 176–196.

Motoyoshi, Y. & Hensen, B. J. (2001). F-rich phlogopite stability in ultra-high-temperature metapelites from the Napier Complex, East Antarctica. *American Mineralogist* **86**, 1404–1413.

Osanai, Y., Toyoshima, T., Owada, M., Tsunogae, T., Hokada, T., Crowe, W. A. & Kusachi, I. (2001). Ultrahigh temperature sapphirine–osumilite and sapphirine–quartz granulites from Bunt Island in the Napier Complex, East Antarctica:—reconnaissance estimation of *P–T* evolution. *Polar Geoscience* **14**, 1–24.

Patiño Douce, A. E. & Johnston, A. D. (1991). Phase equilibria and melt productivity in the pelitic system: implications for the origin of peraluminous granitoids and aluminous granulites. *Contributions to Mineralogy and Petrology* **107**, 202–218.

Pichavant, M., Montel, J.-M. & Richard, R. L. (1992). Apatite solubility in peraluminous liquids: experimental data and an extension of the Harrison–Watson model. *Geochimica et Cosmochimica Acta* **56**, 3855–3861.

Roy, A. J., Grew, E. S. & Yates, M. G. (2003) Wagnerite, apatite and biotite in granulite facies rocks of the Napier complex, Enderby Land, Antarctica; the role of halogens. *Geological Society of America, Abstracts with Programs* **35**(6), 327–328.

Ryan, J. G. (2002). Trace-element systematics of beryllium in terrestrial materials. In: Grew, E. S. (ed.) *Beryllium: Mineralogy, Petrology, and Geochemistry*. *Reviews in Mineralogy and Geochemistry* **50**, 121–145.

Sandiford, M. (1985). The metamorphic evolution of granulites at Fyfe Hills; implications for Archaean crustal thickness in Enderby Land, Antarctica. *Journal of Metamorphic Geology* **3**, 155–178.

Sandiford, M. & Wilson, C. J. L. (1984). The structural evolution of the Fyfe Hills–Khmara Bay region, Enderby Land, East Antarctica. *Australian Journal of Earth Sciences* **31**, 403–426.

Sandiford, M. & Wilson, C. J. L. (1986). The origin of Archaean gneisses in the Fyfe Hills region, Enderby Land; field occurrence, petrography and geochemistry. *Precambrian Research* **31**, 37–68.

Sawyer, E. W. (1987). The role of partial melting and fractional crystallization in determining discordant migmatite leucosome compositions. *Journal of Petrology* **28**, 445–473.

Sawyer, E. W. (1994). Melt segregation in the continental crust. *Geology* **22**, 1019–1022.

Sawyer, E. W. (2001). Melt segregation in the continental crust: distribution and movement of melt in anatectic rocks. *Journal of Metamorphic Geology* **19**, 291–309.

Shaw, D. M., Truscott, M. G., Gray, E. A. & Middleton, T. A. (1988). Boron and lithium in high-grade rocks and minerals from the Wawa–Kapuskasing region, Ontario. *Canadian Journal of Earth Sciences* **25**, 1485–1502.

Sheraton, J. W. (1980). Geochemistry of Precambrian metapelites from East Antarctica: secular and metamorphic variations. *BMR Journal of Australian Geology and Geophysics* **5**, 279–288.

Sheraton, J. W. & Black, L. P. (1983). Geochemistry of Precambrian gneisses: relevance for the evolution of the East Antarctic Shield. *Lithos* **16**, 273–296.

Sheraton, J. W., Tingey, R. J., Black, L. P., Offe, L. A. & Ellis, D. J. (1987). Geology of an unusual Precambrian high-grade metamorphic terrane—Enderby Land and western Kemp Land, Antarctica. *Australia Bureau of Mineral Resources, Geology and Geophysics Bulletin* **223**, 1–51.

Smith, M. S., Dymek, R. F. & Schneiderman, J. S. (1992). Implications of trace element geochemistry for the origin of cordierite–orthoamphibole rocks from Orijärvi, SW Finland. *Journal of Geology* **100**, 545–559.

Steele, I. M., Hutcheon, I. D. & Smith, J. V. (1980). Ion microprobe analysis of plagioclase feldspar ($Ca_{1-x}Na_xAl_{2-x}Si_{2+x}O_8$) for major, minor, and trace elements. In: Beaman, D. R., Ogilvie, R. E. & Wittry, D. B. (eds) *8th International Congress on X-ray Optics and Microanalysis*. Midland, MI: Pendell, pp. 515–525.

Stevens, G., Clemens, J. D. & Droop, G. T. R. (1997). Melt production during granulite-facies anatexis: experimental data from 'primitive' metasedimentary protoliths. *Contributions to Mineralogy and Petrology* **128**, 352–370.

Taylor, S. R. & McLennan, S. M. (1995). The geochemical evolution of the continental crust. *Reviews of Geophysics* **33**, 241–265.

Vielzeuf, D. & Holloway, J. R. (1988). Experimental determination of the fluid-absent melting relations in the pelitic system: consequences for crustal differentiation. *Contributions to Mineralogy and Petrology* **98**, 257–276.

Vielzeuf, D. & Montel, J. M.. (1994). Partial melting of metagreywackes. Part I. Fluid-absent experiments and phase relationships. *Contributions to Mineralogy and Petrology* **117**, 375–393.

White, R. W. & Powell, R. (2002). Melt loss and the preservation of granulite facies mineral assemblages. *Journal of Metamorphic Geology* **20**, 621–632.

Wolf, M. B. & London, D. (1994). Apatite dissolution into peraluminous haplogranitic melts: an experimental study of solubilities and mechanisms. *Geochimica et Cosmochimica Acta* **58**, 4127–4145.